Real-time Measurements of Secondary Organic Aerosol Formation and Aging from Ambient Air in an Oxidation Flow Reactor in the Los Angeles Area

Amber M. Ortega[1,2], Patrick L. Hayes[3], Zhe Peng,[1,4], Brett B. Palm[1,4], Weiwei Hu,[1,4], Douglas A. Day[1,4], Rui Li,[1,2,5,*] Michael J. Cubison[1,4,+], William H. Brune[6], Martin Graus[1,5,++], Carsten Warneke[1,5], Jessica B. Gilman[1,5], William C. Kuster[1,5,^],Joost de Gouw[1,5], Cándido Gutiérrez-Montes[7], and Jose L. Jimenez[1,4]

[1]Cooperative Institute for Research in the Environmental Sciences, University of Colorado, Boulder, CO, USA
[2]Department of Atmospheric and Oceanic Sciences, University of Colorado, Boulder, CO, USA
[3]Department of Chemistry, Université de Montréal, Montreal, Quebec, Canada
[4]Department of Chemistry and Biochemistry, University of Colorado, Boulder, CO USA
[5]Chemical Sciences Division, NOAA Earth System Research Laboratory, Boulder, CO, USA
[6]Department of Meteorology, Pennsylvania State University, University Park, PA, USA
[7]Departamento de Ingeniería, Mecánica y Minera, Universidad de Jaen, Jaen, Spain
[*]now at Markes International Inc., Cincinnati, OH 45242
[+]now at: Tofwerk AG, Thun, Switzerland
[++]now at: Institute of Meteorology and Geophysics, University of Innsbruck, Innsbruck, Austria
^now retired

Abstract

Field studies in polluted areas over the last decade have observed large formation of secondary organic aerosol (SOA) that is often poorly captured by models. The study of SOA formation using ambient data is often confounded by the effects of advection, vertical mixing, emissions, and variable degrees of photochemical aging. An Oxidation Flow Reactor (OFR) was deployed to study SOA formation in real-time during the California Research at the Nexus of Air Quality and Climate Change (CalNex) campaign in Pasadena, CA, in 2010. A high-resolution aerosol mass spectrometer (AMS) and a scanning mobility particle sizer (SMPS) alternated sampling ambient and reactor-aged air. The reactor produced OH concentrations up to 4 orders of magnitude higher than in ambient air. OH radical concentration was continuously stepped, achieving equivalent atmospheric aging of 0.8 days–6.4 weeks in 3 min of processing every 2 hrs. Enhancement of OA from aging showed a maximum net SOA production between 0.8–6 days of aging with net OA mass loss beyond 2 weeks. Reactor SOA mass peaked at night, in the absence of ambient photochemistry and correlated with trimethylbenzene concentrations. Reactor SOA formation was inversely correlated with ambient SOA and O_x, which along with the short-lived VOC correlation, indicates the importance of relatively reactive (τ_{OH} ~0.3 day) SOA precursors (most likely semivolatile and intermediate volatility species, S/IVOC) in the greater Los Angeles Area.. Evolution of the elemental composition in the reactor was similar to trends observed in the atmosphere (O:C vs. H:C slope ~ -0.65). Oxidation state of carbon (OSc) in reactor SOA increased steeply with age and remained elevated (OS_C ~2) at the highest photochemical ages probed. The ratio of OA in the reactor output to excess CO (ΔCO, ambient CO above regional background) vs. photochemical age is similar to previous studies at low to moderate ages and also extends to higher ages where OA loss dominates. The mass added at low-to-intermediate ages is due primarily to condensation of oxidized species, not heterogeneous oxidation. The OA decrease at high photochemical ages is dominated by heterogeneous oxidation followed by fragmentation/evaporation. A comparison of urban SOA formation in this study with a similar study of vehicle SOA in a tunnel supports the dominance of vehicle emissions in urban SOA. Pre-2007 SOA models underpredict SOA formation by an order of magnitude, while a more recent model performs better but overpredicts at higher ages. These results demonstrate the value of the reactor as a tool for *in situ* evaluation of the SOA formation potential and OA evolution from ambient air.

1 Introduction

Atmospheric aerosols are the most uncertain aspect of the climate radiative forcing (Myhre et al., 2013), and have negative impacts on human health (Pope et al., 2002) and visibility (Watson, 2002). Organic aerosol (OA) represents a large fraction of fine particle mass (Murphy et al., 2006; Zhang et al., 2007) and is the least-characterized component of submicron aerosol due to its complexity and wide variety of emission sources and atmospheric processes (Jimenez et al., 2009). OA can be emitted directly into the atmosphere from primary OA sources (POA), such as traffic or biomass burning, or formed through atmospheric processing as secondary OA (SOA). SOA can be formed when volatile organic compounds (VOCs) react with atmospheric oxidants such as ozone and hydroxyl radicals (O_3 and OH), to form less-volatile products that can partition into the aerosol phase (Pankow, 1994; Donahue et al., 2006), as well as through heterogeneous and multiphase processes (Ervens et al., 2011). An improved understanding of the sources, atmospheric processes, and chemical properties of SOA is necessary to constrain and predict current impacts on human health and climate as well as shifting impacts with changing climate and emissions (Hallquist et al., 2009).

SOA concentrations are typically underestimated by over an order of magnitude when pre-2007 models are applied in urban regions (Volkamer et al., 2006; de Gouw and Jimenez, 2009; Hodzic et al., 2010; Morino et al., 2014; Hayes et al., 2015). These “traditional” models treated SOA formation as partitioning of semivolatile products from gas-phase oxidation of VOCs, using aerosol yields and saturation concentrations from older environmental chamber studies. More recently updated models have incorporated (higher) SOA yields from VOCs from more recent chamber studies. Some studies have used artificially higher yields based on “aging” of the VOC products, although these are unconstrained by chamber studies (e.g. Tsimpidi et al., 2010), or increased yields to account for losses of semivolatile gases to chamber walls (Zhang et al., 2014; Hayes et al., 2015). Donahue et al. (2006) developed the volatility basis set (VBS) formalism for modeling OA partitioning, in which organic species are distributed into volatility bins, which has been adopted by many SOA modeling schemes. Semi-volatile and intermediate volatility compounds (S/IVOCs) have been identified as additional precursors that were not considered in traditional models (Robinson et al., 2007). These updated approaches have been applied to several urban datasets leading to better closure between measured and modeled bulk OA, but have resulted in other problems such as several-fold overpredictions of SOA at long aging times (>1 day; Dzepina et al., 2011; Hayes et al., 2015; Zhang et al., 2015) or SOA that is much too volatile compared to observations (Dzepina et al., 2011). These models remain under-constrained, and it is unclear whether the updated models increase predicted SOA formation for the right reasons. Targeted field studies in urban areas, with sufficient constraints and with novel approaches for focused investigation of SOA formation, are essential for continued model testing and improvement.

In order to characterize the SOA formation potential of urban emissions, a rapid field deployable experimental method is needed, so that potentially rapid changes of ambient SOA formation potential can be captured.. The “Potential Aerosol Mass” (PAM) oxidation flow reactor (OFR), was developed by Kang et al., (2007; 2011), and used in many laboratory experiments and recent field studies. It is a small flow reactor that exposes air samples to high oxidant levels (100-10,000 times atmospheric concentrations) with short residence time (<5 min). Recent work with the reactor has examined SOA yield, oxidation, and physicochemical changes using single precursors or simple mixtures in laboratory experiments, producing results similar to environmental chamber experiments (Massoli et al., 2010; Kang et al., 2011; Lambe et al., 2011a; Lambe et al., 2011b;

Bruns et al., 2015). SOA yields in the reactor are comparable or somewhat lower than for similar OH exposures in large environmental chambers, which has been suggested to be due to the short residence time of the reactor not being sufficient to allow complete condensation of semivolatiles (Lambe et al., 2015) or increased wall losses of gas-phase species due to the higher surface area to volume ratios of the reactor (Bruns et al., 2015). OH oxidation of alkane SOA precursors in the reactor show the effect of functionalization (oxygen addition) and fragmentation (carbon loss) reactions (Lambe et al., 2012). Recent reactor application to aging of biomass burning smoke showed that total OA after reactor oxidation was on average 1.42±0.36 times the initial primary OA (POA) with similar aging of biomass burning tracers to that observed in aircraft measurements (Cubison et al., 2011; Ortega et al., 2013). Aging measurements of vehicular exhaust using the reactor in a highway tunnel in Pittsburgh, PA indicated peak SOA production after 2.5 days of atmospheric equivalent photochemical aging (at OH = 3×10^6 molec cm^{-3}) and concluded the chemical evolution of the OA inside the reactor appears to be similar to that observed in the atmosphere (Tkacik et al., 2014). Other studies also show that the reactor produces SOA with characteristics similar to that formed in the atmosphere for crude oil evaporation (Bahreini et al., 2012a; Li et al., 2013). The radical chemistry in the reactor has been recently characterized (Li et al., 2015; Peng et al., 2015).Thus, the reactor is a useful tool for elucidating SOA formation processes under field conditions where utilizing large-scale environmental chambers is not practical and/or if a higher degree of aging is targeted.

Due to meteorological conditions (e.g. diurnal fluctuations in land-sea breeze patterns with weak synoptic forcing) and topography (e.g. the surrounding coastal mountain ranges) ventilation of air in the greater Los Angeles area (LA-Basin) can be limited, historically resulting in high pollution levels. Several field campaigns have investigated SOA in the LA-Basin, including the 2005 Study of Organic Aerosol at Riverside (SOAR; Docherty et al., 2011) and the 2009 Pasadena Aerosol Characterization Observatory (PACO; Hersey et al., 2011). These studies identified SOA as a major fraction of total OA in the LA Basin in the summer, consistent with findings in previous urban field campaigns (Volkamer et al., 2006; de Gouw and Jimenez, 2009). This situation is in contrast to previous studies in this region which reported that primary OA was higher than SOA, other than during severe photochemical smog episodes; however, these estimates were likely affected by apportionment biases or the greatly underestimated SOA production of traditional models (Docherty et al., 2008).

The 2010 California Research at the Nexus of Air Quality and Climate Change (CalNex) was a multiplatform large-scale field study, which utilized ground sites at Bakersfield and Pasadena, California, NOAA WP-3D and Twin Otter aircraft, and the research ship *R/V Atlantis* (Ryerson et al., 2013). In this study, we measured submicron aerosol size and composition alternately for ambient air and for ambient air that had been aged in an oxidation flow reactor by systematically changing the OH exposure. This work is compared to the previous literature but extends beyond it with the new information provided by the *in situ* aging studies. By combining results from the ambient aerosol and aged ambient aerosol measurements, we provide a stronger test of current SOA models, since they can now be compared with data from a much wider range of photochemical ages. In order to characterize the SOA formation potential of urban emissions, a field deployable experimental method is needed that is capable of rapid operation to allow examination of the variable potential of changing air masses.

2 Experimental Methods

2.1 CalNex Field Campaign

The work in this study will focus on measurements from the Pasadena ground site during CalNex. The Pasadena site was located on the California Institute of Technology (Caltech) campus in Pasadena, CA (34.1406 N, 118.1225 W, 236 m above mean sea level); the location, airmass transport, and key measurements have been described in detail previously (Washenfelder et al., 2011; Hayes et al., 2013). The measurement period for our reactor study is 29 May–10 June 2010, hereafter referred to as the "sampling period." Meteorological conditions, including prevailing winds, boundary layer height, temperature, and relative humidity information are summarized by Washenfelder et al. (2011) and Hayes et al. (2013). An overview of the 2010 CalNex field campaign (Ryerson et al., 2013) and aerosol observations at the Pasadena Supersite (Hayes et al., 2013) can be found in previous publications. A gas-chromatography mass spectrometer (GC-MS) from NOAA was located at the same field site (Hayes et al., 2013; Warneke et al., 2013) and used for VOC measurements reported in this study. The NOAA WP-3D research aircraft sampled *in situ* meteorological, trace gas, and aerosol conditions aloft during CalNex (Bahreini et al., 2012b; Ryerson et al., 2013). Non-refractory submicron aerosol composition measurements aboard the NOAA WP-3D were made using an Aerodyne compact time-of-flight aerosol mass spectrometer (C-ToF-AMS, Drewnick et al., 2005). Details of operation, analysis, and quantification can be found in Bahreini et al. (2012b).

2.2 Oxidation Flow Reactor

To study SOA formation and OA aging *in-situ*, we deployed a Potential Aerosol Mass (PAM) oxidation flow reactor (Kang et al., 2007; Kang et al., 2011) at the Pasadena ground site. Fig. 1a shows a diagram of the operational setup. The reactor and ambient sample lines were located adjacent to one another, on the roof of the instrument trailer at 7.2 meters above ground (Fig. 1b). Ambient air was continuously sampled in an open flow-through configuration via a 14-cm diameter opening with coarse-grid mesh screen coated with an inert silicon coating (Sulfinert by SilcoTek, Bellefonte, PA). The mesh was designed to block debris and insects, as well as break up large eddies while allowing VOCs and oxidized gases to be sampled efficiently. This configuration, with no inlet, was chosen because of the observation of reduced SOA formation when any inlet and/or an inlet plate was used in a previous experiment (Ortega et al., 2013). The reactor output was measured by an AMS (described below), a scanning-mobility particle sizer (SMPS, TSI Inc., Model 3936 with TSI 3010 CPC), and an O_3 monitor (2B Technologies, Model 205). The uncertainty in the O_3 measurement is +/- 1.5 ppb or 2% of the measurement, whichever is greater. Fast switching valves were used to automatically alternate AMS and SMPS sampling between the reactor and unperturbed ambient sample line every 5 minutes. Bypass lines were used to maintain constant flow in both the reactor and ambient sample lines while instrumentation was sampling the other channel, to avoid artifacts due to particle or gas losses or re-equilibration that could occur if flow had been stagnant in the lines or modulated in the reactor. The configuration with the large inlet strongly reduces recirculation in the reactor and narrows the residence time distribution (RTD) (Fig. S1). To further reduce the width of the RTD, output flow was sampled from both a central stainless steel 1/4 inch OD tube at 2.0 L min^{-1} for aerosol measurements and a 3/8 inch OD PTFE Teflon perforated ring with 14 cm diameter for gas-phase measurements at 2.4 L min^{-1}. In addition, Peng et al. (2015) has shown that variations in the residence time distribution in the OFR had limited impact on the estimated OH_{exp}.

The total flow rate through the reactor was 4.4 lpm corresponding to a residence time of 3 min. The reactor was used to expose ambient air to high levels of OH and O_3, produced when UV light from two low-pressure mercury lamps (model no. 82-9304-03, BHK Inc., with discrete emission peaks at 254 and 185 nm) initiated O_2, H_2O and O_3 photochemistry. This mode of operation is referred to as OFR185, and OH is formed from both H_2O and O_3 photolysis (Li et al., 2015). In this mode O_3 is formed in the reactor but is not added to the reactor, contrary to the OFR254 mode that has been used mainly in laboratory studies (Peng et al., 2015). Given that most known urban SOA precursors do not react with O_3 (e.g. Hayes et al., 2015), d using we expect OH to dominate the observed SOA formation. Consistent with this, no SOA was formed in test experiments during CalNex when ambient air was exposed to O_3 only without OH. We use the term “aging” to refer to the combined effect of OH, O_3, and light exposure in the flow reactor, although reactions in the reactor are understood to be dominated by OH under typical operating conditions (Peng et al., 2016). Peng et al. (2016) have investigated the possibility of photolysis of gases and aerosol species under the OFR conditions. OH reaction dominated the fate of all gases studied. Under most conditions in this study, photolysis was estimated to be responsible for only several percent of the fractional destruction of the gas-phase primary species most susceptible to it (aromatic species) even if photolysis quantum yield was assumed to be 1. The upper limit of the fractional destruction of possible oxidation intermediates was ~x2 that of primary species. Photolysis of SOA already present in the atmosphere may have played some role at the medium and high UV settings studied here when assuming upper limit quantum yields. However photolysis e-fold decays in the reactor are estimated to be orders-of-magnitude lower than for the atmosphere for equivalent OH exposures.

The intensity of aging was continuously stepped by computer-controlled lamp power supplies (custom made transformers from BHK Inc., controlled via Labview using a National Instruments analog output board NI USB-6501), resulting in systematic stepping of lamp input voltage from

50–110 VAC. This voltage stepping modulates the photon flux and consequently the OH concentrations in the reactor (Li et al., 2015). The lights are housed in Teflon sleeves which are purged with N_2 gas to remove heat and avoid exposing the lamp surfaces to O_3 or other oxidants. When operated at full power the lights result in an increase of ~2°C above ambient conditions. Given the low volatility of ambient OA (Huffman et al., 2009; see Fig. S12 and associated discussion below), little OA evaporation is expected in the reactor due to this heating.

Oxidant concentrations in the reactor were stepped in 20-minute intervals, through six levels (including lights off, i.e. no added oxidants) comprising a two-hour cycle (Fig. 2). Only data from the last five minutes of each 20-minute period are used, to avoid including reactor transient periods. Thus, five full residence times have elapsed after changes to the UV lights and before starting to sample reactor outputs, to allow full replacement of the contents of the reactor. As lamp intensity increased, O_3 and OH concentrations increased in the reactor, and resultant OA concentrations were measured from the reactor after oxidant perturbation as seen in Fig. 2. To correct for the effect of particle losses we compared concentrations measured in the reactor output when UV lights are turned off with those measured through the ambient inlet. The loss of particle mass in this aluminum reactor is small, of the order of a few percent of the ambient concentrations (see also Palm et al., 2016). Losses in an OFR with a quartz body were observed to be ~35% in a previous study (presumably due to nearly complete loss of charged particles), which led to our use of the all-aluminum reactor. A time-dependent correction factor was estimated by comparing each reactor output measurement (for each period when the lights were off) with the average of the two ambient measurements immediately before and after. This correction is interpolated in time and applied to all reactor output measurements with lights on. The resulting average correction was +5.8 %. Although losses may have some size dependence, given the broad distributions covering the same size ranges for both ambient air and OFR output, and the small magnitude of the correction, this effect has not been considered in detail.

The OH exposure (OH_{exp}, OH concentration integrated over the reactor residence time) achieved in this study is primarily a function of lamp photon flux (at 185 and 254 nm), residence time, and ambient H_2O concentration and OH reactivity (Li et al., 2015; Peng et al., 2015). OH_{exp} was estimated using an equation developed by multivariate fitting of the output from a kinetic model of reactor (OFR185) operation, and verified against data from several field and laboratory experiments including CalNex (Li et al., 2015). Data from the decay of ambient SO_2 in the OFR during CalNex, which was only reliable during periods with higher ambient SO_2 concentrations (> 1 ppbv), was used to verify the OH_{exp} estimation equation. The equation uses ambient H_2O concentration, reactor output O_3 concentrations, residence time, and ambient OH reactivity from collocated measurements (total OH reactivity measurement from the Stevens Group, Indiana University; in this method there is no assumption about the reactivity constituents). According to this equation, internal OH_{exp} in the reactor typically ranged from 1.1×10^{11}–5.8×10^{12} molec. cm^{-3} s, 0.8 days–6.4 weeks of photochemical age assuming 24-hr average ambient OH concentrations of 1.5×10^{6} molec. cm^{-3} (Mao et al., 2009). The uncertainty in the calculated OH_{exp} is estimated to be a factor of 3 (Li et al., 2015; Peng et al., 2015). "Total photochemical age" refers to the sum of ambient photochemical age and reactor internally-generated photochemical age, used throughout this work unless otherwise specified. Ambient photochemical age is calculated by the ratio of 1,2,4-trimethylbenzene to benzene (Borbon et al., 2013), using collocated gas-phase measurements as described in Hayes et al. (2013). Subsequent figures use total photochemical age in day-units applying the average OH concentration of 1.5×10^{6} molec. cm^{-3}. During CalNex, OH concentrations averaged as high as 4×10^{6} molec. cm^{-3} during the daytime, from concurrent OH reactivity estimates. Since a significant part of SOA formation happens during the first few hours after emission, the 0.8 day minimum photochemical age probed with the reactor would correspond to ~0.3 days at the peak OH concentration observed during CalNex.

2.3 Particle Measurements

Particle concentration and composition were analyzed with a high-resolution time-of-flight aerosol mass spectrometer (HR-ToF-AMS, abbreviated as AMS hereafter; Aerodyne Research, Billerica, MA; DeCarlo et al., 2006; Canagaratna et al., 2007). The ambient measurement setup, instrument intercomparisons, scientific results, and their interpretation are reported in Hayes et al. (2013). he high-resolution (HR) fragmentation table (Aiken et al., 2008) and peak fitting (DeCarlo et al., 2006) were applied to the reactor measurements with no additional adjustments beyond those performed for the ambient CalNex data by Hayes et al. (2013). The elemental analysis of OA (resulting in oxygen-to-carbon ratio, O:C, and hydrogen-to-carbon ratio, H:C) was performed using the “improved-ambient” method published by Canagaratna et al. (2015) for both reactor and ambient measurements, which increases O:C on average by 27% and H:C on average by 11% over the previous “Aiken ambient” method (Aiken et al., 2008). Details of the quantification of AMS reactor measurements (i.e. collection efficiency, inlet and particle lens losses) and intercomparison with the SMPS are discussed in supplementary Section S1 (Figs. S2-S6). Hayes et al. (2015) performed a modeling study comparing the ambient AMS OA measurements with several box and 3-D SOA models. Here, we only discuss the modifications in post-processing and data analysis necessitated by the alternating sampling of the reactor output.

2.4 Fate of Low-Volatility Organic Gases in the Reactor

As organic gases are oxidized, they can form lower vapor pressure products, low-volatility organic compounds (LVOC). Semivolatile organic compounds (SVOC) will also be formed, but we focus this discussion on LVOC for several reasons. As shown in Figure S12 (discussed in Section 4.4), the volatility distribution of the SOA present during CalNex shows very limited importance of SVOCs as SOA constituents. Second, discussion and modeling of LVOC fate in the reactor is conceptually simpler. Third, the amount of SOA formed in reactor is significantly higher than can be explained by the speciated precursors, consistent with other studies (Palm et al., 2016). The assumption of LVOCs results in higher SOA formation than if SVOC were assumed, and is thus a the most conservative assumption in terms of closure of measured vs. predicted SOA. Thus adding complexity to the loss model for species that are likely of limited importance was a lower priority for our study.. In the atmosphere, the dominant fate of these LVOC is condensation on aerosols, as OH lifetimes and dry deposition time scales are slower (Donahue et al., 2013; Knote et al., 2015). However, given the limited residence time, high surface/volume ratio, and the high oxidant concentrations in the OFR, other LVOC fates can be competitive with condensation on aerosols. LVOC in the reactor can either condense on aerosols, be lost due to condensation on the reactor walls, react further with OH resulting in condensable or non-condensable products, or exit the reactor in the gas phase to condense on the sampling line walls. Aerosol sampling instruments only measure the LVOC that condense on aerosols in the reactor. Given the short residence time and high OH_{exp} of the reactor, SOA formation could be underestimated due to these competing fates. To account for vapor losses, we follow the method detailed in Palm et al. (2016), using McMurry and Grosjean (1985) for wall loss estimation. The method of Pirjola et al. (1999) is used for estimating organic gas condensation to aerosols based on the measured SMPS size distributions with the Fuchs-Sutugin correction for gas diffusion in the transition regime (Seinfeld and Pandis, 1998). It is assumed that products after five oxidation steps with OH at k_{OH} = 1 x 10^{-11} molec cm^{-3} s^{-1} are lost (fragmented and too volatile to condense). We note that 56% (97%) of the initial molecules will have undergone five oxidation steps after an OH_{exp}= 5×10^{11} (1×10^{12}) molec. cm^{-3} s. This is used to simulate a typical C_{10} VOC oxidation in the reactor. Parameters used include the measured surface-area-to-volume ratio (A/V) of the reactor (25 m^{-1}), a coefficient of eddy diffusion k_e approximated as 0.0036 s^{-1}, and a diffusion coefficient D = 7×10^{-6} m^2 s^{-1}, corresponding approximately to the diffusivity of a molecule with a mass of 200 g mol^{-1}. The analyses leading to the correction terms were developed in Palm et al. (2016) and are applied here. As Palm et al. (2016) is now published in final form in ACP, we refer readers to that manuscript for the full details of the method.

At OH_{exp} lower than 1×10^{12} molec cm^{-3} s (∼ 10 days) the dominant LVOC fate (50–75%) is condensation to the aerosol (see Fig. S7). At higher OH_{exp}, the fate of organic gases is dominated (>45%) by loss to reaction with OH rather than condensing on aerosol. LVOC lost to the walls (~7%) or exiting the reactor (~2%) play only small roles under the conditions of this study, due to the relatively high ambient aerosol surface area. The amount of SOA formed in the reactor is corrected for the fraction of SOA that condense on the aerosol by fitting a line to the calculated fraction of LVOCs that condense on aerosol and dividing the measured SOA formed in the reactor by the fitted fraction of LVOCs that were lost by condensation on the aerosol (Fig. S7). This correction is a minimum at low to moderate ages, and highest at longest ages where net OA production is lowest (Sect. 3.2). Thus, the maximum net SOA production was typically corrected by a factor of 1.2. At increasing ages, where OA loss due to heterogeneous oxidation begins to dominate over gas-phase oxidation, it becomes unfeasible to apply the correction, as the net OA enhancement in the reactor is negative. Thus, correction is applied when reactor-measured OA is greater than ambient OA (relative OA enhancement ratio, ER_{OA} = reactor OA / ambient OA, $ER_{OA}>1$; and the absolute OA enhancement factor, ΔOA Mass = reactor OA – ambient OA, ΔOA Mass>0, Sect. 3.2).

3 Results and Discussion

3.1 Observations

The time series of the reactor sample period is shown in Fig. 3a. The ambient aerosol during the first third (30 May–3 June 2010) of the measurement period is characterized by OA dominance, while the remaining two-thirds of the period (3–11 June 2010) is characterized by high concentrations of OA and nitrate, moderate sulfate and ammonium, and low chloride, with a marked diurnal cycle. This second period was strongly affected by in-basin pollution and is the most useful in terms of studying urban SOA formation (Hayes et al., 2013). The precursors that are expected to be important contributors to SOA at this location include aromatic VOCs and semivolatile and intermediate volatility species (mostly alkanes and aromatics), with low importance for biogenic species (Hayes et al., 2015).

A 24-h snapshot of the time series of ambient and reactor data is shown in Fig. 3b. This period is representative of the diurnal profiles observed from 3–9 June 2010. The oscillations (zig-zag pattern) in reactor output concentrations are due to OH_{exp} stepping as shown in Fig. 2. Day and night periods are highlighted to indicate the period of inactive (20:00–8:00) and active ambient photochemistry (8:00–20:00) in Fig. 3b. Ambient nitrate and ammonium concentrations peak in early morning hours before sunrise, while OA peaks in the late afternoon, during the most photochemically active part of the day. Hayes et al. (2013) attribute this organic aerosol temporal pattern to the formation of fresh urban SOA as the LA-plume undergoes ~0.3 days of photochemical aging during transport to our field location, which is considered a receptor site as it experienced a strong impact from aged urban emissions. However, OA enhancement in the reactor peaked during night, ~12 h before the ambient OA peak. The nighttime reactor-aged OA mass peaks at approximately the same concentration as the following day's ambient OA concentration, suggesting the reactor's potential for estimating the next day's OA concentrations. A more quantitative evaluation of this potential is discussed below (Sect. 4.1. and Figure 9). While this peak likely occurs at OH_{exp} higher than observed the following day, the similar OA mass added highlights the potential for further develop of the reactor as a predictive tool. Daytime reactor-aged OA mass shows very limited enhancement above the ambient OA mass, suggesting that the precursors for SOA formation have been mostly depleted in ambient air. The nighttime reactor-aged OA mass peaks at approximately the same concentration as the following day's ambient OA concentration, suggesting the reactor's potential for estimating the next day's OA concentrations. A more quantitative evaluation of this potential is discussed below (Sect. 4.1. and Figure 9). The fact that the inorganic components are enhanced in the reactor is not surprising but expected. SO_2 and NO_x in ambient air are expected to be oxidized to H_2SO_4 and HNO_3 by the OH in the reactor, and can then condense onto the aerosols (together with ambient NH_3 for HNO_3). See e.g. Kang et al. (2007) and Li et al. (2015) for further details. Figure 3c shows the average speciated contribution to total aerosol for ambient and the reactor (excluding dark reactor periods, "lights off" periods, periods are included only if OH_{exp} > ambient), indicating overall enhancement of all species from reactor aging with very similar composition to ambient aerosol.

Observations of the OA size distributions indicate reactor aging does not significantly shift the size of the accumulation mode for the average of nighttime ambient and three different reactor age ranges (age ~ ambient, 3.7 days, and 23.5 days), from 2–9 June 2010 (Fig. S8). The reactor size distribution changes in intensity and shape are most pronounced during low ages (~3.7 days and lower), with an enhanced smaller size mode (d_{va} ~80 nm). While many daytime/nighttime average size distributions and age ranges were explored, only ages at or below a few days at nighttime showed significant enhancement of small particle sizes. Highest ages (>14 days) show overall decrease in concentration across all size bins with the size of the accumulation mode unchanged from ambient within the uncertainty of the measurement. Given the high concentrations of large particles in this urban environment, we expect aging to enhance organic aerosol by condensation of semi- and low-volatile compounds on existing particles to dominate over new particle formation and growth. Reactor results are indicative of this process, although they also indicate the effect of new particle formation and/or of nanoparticle growth at lower OH exposures.

3.2 Aerosol Enhancements

Investigating reactor perturbation of ambient OA allows quantification of both relative and absolute OA changes vs. OH_{exp}. The relative OA enhancement ratio, ER_{OA}, and the absolute OA enhancement factor, ΔOA Mass, are plotted vs. OH_{exp} in Fig. 4a and Fig. 4b respectively for the sample period. OA mass is enhanced up to four times from ambient OA, with the majority of maximum ER_{OA} peaking around a factor of two increase. OA enhancement peaks and plateaus between 0.8–6 days of OH aging, then decreases at higher aging, eventually showing net OA loss beyond two weeks of aging. When separated into daytime and nighttime ER_{OA} and ΔOA mass (Fig. 4), the qualitative trends are the same in both cases, but OA was more enhanced from reactor aging during nighttime by 5 μg m^{-3}, or a factor of 1.7x of ambient. A smaller enhancement is observed during the day ~2 μg m^{-3}, or a factor of 1.2x of ambient, while at > 2 weeks of aging, day and night observations closely overlap, with a decrease up to ~2.5 μg m^{-3}, or a factor of 0.5x of ambient.

The substantial difference between day- and nighttime enhancements can be explained as during the night the boundary layer is shallow and reactive precursors accumulate due to the absence of ambient photochemistry, with lower ambient photochemical ages of ~0.1 day (Hayes et al., 2015) and minimal loss mechanisms as the dominant urban VOCs do not react with O_3 or NO_3 (other than a small concentration of monoterpenes). In contrast, during the day reactive precursors in ambient air are depleted due to reaction with OH. Transport times from downtown LA, the dominant precursor source region impacting Pasadena, is ~0.5 days (Washenfelder et al., 2011; Hayes et al., 2013), with ambient photochemical ages reaching ~0.3 days. Thus most of the SOA precursors that can become SOA already have by the time the air was sampled in Pasadena and only about 20% more SOA could be produced from the precursors that remained. The trends in Fig. 4 indicate increased oxidation transitioning from a dominance of functionalization reactions and condensation at low-to-moderate exposures, to fragmentation-dominated reactions and evaporation of reaction products at the highest photochemical ages. Fragmentation can occur in the gas phase by reactions of SVOCs with OH, leading to non-condensable products and decreasing SOA formation. Fragmentation can also be due to heterogeneous oxidation of existing OA, producing more volatile species that may evaporate leading to OA mass loss. Discussion of the relative importance of these processes for this study is presented in Section 4.4 below.

3.3 Gas-Phase Observations

3.3.1 Odd Oxygen (O_x) Relation to SOA Formation

The day-night difference observed in both ER_{OA} and ΔOA mass merits examination of the relationship with ambient odd-oxygen, O_x (O_3 + NO_2). Ambient O_x correlates with freshly produced SOA in urban areas (Herndon et al., 2008; Wood et al., 2010; Hayes et al., 2013; Morino et al., 2014; Zhang et al., 2015), both resulting from recent photochemistry. For the reactor, oxidants are generated internally and are not dependent on ambient O_x. As seen in Fig. 5, there is a steep inverse relationship between ΔOA mass and ambient O_x, at low to moderate aging (<4 days). As daytime ambient photochemical production of oxidants increases (O_x >50 ppbv), the reactor's SOA formation for moderate aging decreases to a near constant OA mass enhancement (2 μg m^{-3}). At high ages (>14 days), OA mass loss is fairly constant with ambient O_x, which is not surprising since the mechanisms responsible for OA depletion at long ages have little dependence on previous photochemical processing in the atmosphere. As O_x is not itself playing a role in reactor aging, but can be used as a proxy ambient photochemistry, these results further confirm that as the degree of ambient photochemical processing of the sampled air increases (during daytime), SOA production in the reactor becomes more limited, likely due to the depletion of reactive SOA precursors in ambient air, consistent with the conclusions from Fig. 4.

3.3.2 Further Constraints on Urban SOA Formation Timescales from OH Reactivity of Measured VOCs

To further constrain the timescales and precursors of urban SOA formation, ambient and reactor OA data are plotted together with ambient VOCs in Fig. 6. The maximum reactor OA enhancement has a similar diurnal profile to 1,3,5–trimenthylbenzene (TMB). Both TMB and OA enhancement have diurnal profiles that are out of phase with ambient SOA. In contrast, the concentration of benzene shows little correlation with reactor SOA formation in the reactor. The lifetime of TMB by reaction with OH is nearly 2 orders of magnitude shorter, τ_{OH} ~3 hours, $k_{OH} = 5.67\times10^{-11}$, than benzene, τ_{OH} ~6 days, $k_{OH} = 1.22\times10^{-12}$ (Atkinson et al., 2006). The anti-correlation of TMB and reactor enhancement in OA and ambient SOA concentrations suggests that only in the absence of ambient photochemistry, substantial amounts of short-lived SOA precursors are present to produce most of the SOA formed in the reactor. Toluene, a VOC with a lifetime of 1.4 days and $k_{OH} = 5.63\times10^{-12}$ cm^3 molecule^{-1}s^{-1} does not have the same diurnal structure as reactor OA and TMB (Fig. S9). The shape of the diurnal-scale time series in Fig. 6 and S9 can be explained as the sunrises ambient photochemistry begins at sunrise, very short lived precursors, such as TMB, begin decay rapidly due to gas-phase oxidation as well as boundary layer growth. As these gas-phase oxidation products condense, SOA forms and ambient OA reaches its daytime peak. At the daytime ambient OA peak, most of these short-lived precursors have been consumed, thus the reactor only forms an additional 1–2 μg m^{-3} of SOA as opposed to the greater than 10 μg m^{-3} possible when these precursors are allowed to build in a shallow boundary layer and in the absence of photochemical sinks. Note that in the afternoon the boundary layer is significantly deeper than at night, and thus the total afternoon SOA formation potential may not be that different than at night, even though the potential per unit volume of air is much smaller.

The inset in Fig. 6 is a scatter plot of maximum reactor SOA formation (per OH_{exp} cycle) vs. TMB (slope ~52, R^2=0.7). TMB's SOA yield is on the order of 10% (Cao and Jang, 2007). Thus its concentration is insufficient to explain reactor SOA formation by a factor of ~500, though it is not expected to be the sole SOA precursor. This correlation suggests species with a similar source footprint and lifetime as TMB produce most of the urban SOA. Such species likely include semivolatile and intermediate volatility precursors (S/IVOC) that are rarely measured in ambient air (Dzepina et al., 2009; Zhao et al., 2014; Hayes et al., 2015), due to the difficulty in measuring these compounds. A comparison of observed reactor SOA formation with a model that uses all the measured VOCs is discussed in section 4.3 below.

3.4 OA Chemical Composition and Evolution with Aging

The evolution of OA chemical composition upon aging has been the subject of several studies, both for ambient (Heald et al., 2010; Kroll et al., 2011; Ng et al., 2011a; Ng et al., 2011b) and reactor conditions (Kang et al., 2011; Ortega et al., 2013; Tkacik et al., 2014; Lambe et al., 2015). This evolution results in characteristic trends in specific diagrams: AMS fragments f_{44} vs. f_{43}, and H:C vs. O:C. Both diagrams are shown for the CalNex ambient and reactor data in Fig. 7. f_{44} is a tracer for aged OA (fractional organic contribution at *m/z* 44, mostly CO_2^+), while f_{43} (fractional organic contribution at *m/z* 43, mostly $C_2H_3O^+$), due to non-acid oxygenates, with some contribution from $C_3H_7^+$) is a tracer of POA and freshly formed SOA (Ng et al., 2011a). In Figure 7a, ambient and reactor data evolve consistently as f_{44} increases and f_{43} decreases with aging, consistent with previous ambient field observations from multiple field campaigns (Ng et al., 2010). As expected, reactor data with the highest age has the highest f_{44}. Positive Matrix Factorization (PMF) factors from Hayes et al. (2013) lie within ambient observations and data for lower OH_{exp} in the reactor. Reactor data stays within the boundary of flow reactor results from Lambe et al. (2011a) and below the location of oxalic acid, as expected.

The Van Krevelen diagram (H:C vs. O:C) is shown in Fig. 7b and demonstrates results that are very consistent to those of the previous plot. The reactor data follows a similar trend to ambient data, with slopes of -0.64 and -0.68, respectively. A slope between -1 and -0.5 is consistent with the addition of acid and alcohol functional groups without fragmentation or the addition of acid groups with carbon–carbon bond breakage (Ng et al., 2011b). The consistency of ambient and reactor OA aging suggest that the reactor produces similar SOA composition upon aging to that in the atmosphere within the LA-Basin.

Reactor O:C ratios increase with age and span a wider range than ambient observations (O:C up to 1.4). While O:C (and f_{44}) continually increased with additional OH_{exp}, peak reactor OA enhancement is observed at intermediate exposures and O:C ratios (0.8–6 days and O:C ~1.10–1.25), as seen in Fig. 8a. OA mass loss, i.e. $ER_{OA} < 1$, is observed together with the highest O:C ratios at the highest ages, which suggests OA fragmentation by heterogeneous oxidation results in the highest oxygen content remaining in the aerosol. With increasing age, H:C decreases continuously with OH_{exp} (Fig. 8b), with H:C ~1.00–1.15 for the periods of maximum reactor OA enhancement. A qualitatively similar trend is observed in the reactor studies of Lambe et al. (2012) for SOA from OH oxidation of alkane precursors (Fig. 8a) although starting with lower O:C and with a steeper slope at higher ages, and also by Ortega et al. (2013) for aging of biomass burning smoke.

Average carbon oxidation state (OS_C) has been proposed as a metric to characterize the formation and evolution of OA (Kroll et al., 2011). OS_C can be approximated as ~2×O:C–H:C. Figure 8c shows OS_C vs. photochemical age for ambient and reactor data. While ambient OS_C is within the range of previous observed urban/anthropogenic OA, reactor OS_C extends this significantly up to +2.0, consistent with ambient low-volatility OA observations up to +1.9 (Kroll et al., 2011). At the same OH exposure, i.e. 8 days, higher OS_C is observed (~1) for conditions of high reactor SOA production (ER_{OA} ~ 2) compared to no net SOA production (ER_{OA} ~ 1, OS_C ~ 0). The highest values of OS_C are observed for the highest ages, where heterogeneous oxidation leading to OA mass loss dominates. This indicates that heterogeneous oxidation adds substantial oxygen and reduces hydrogen from molecules to the particles to increase OS_C despite overall mass loss.

4 Discussion

4.1 Evolution of Urban OA with Photochemical Age

The identity of the SOA precursors responsible for urban SOA formation remains unclear. Combustion emissions such as those from vehicles are thought to be a major source of urban SOA (e.g. Hayes et al., 2015), and urban non-combustion sources of SOA precursors, if important, are finely spatially intermingled with combustion sources. CO is often used as a tracer of the initial concentration of urban SOA precursors in an airmass and thus allow an implicit correction for dilution occurring in parallel with aging. For this reason, the ratio of OA to CO concentration (above background level) vs. photochemical age is often used to investigate the evolution of urban SOA (de Gouw et al., 2005; DeCarlo et al., 2010).

Figure 9 shows the results of this analysis for our reactor and ambient measurements. Background CO during CalNex-LA is on average ~105 ppb (ranging from 85—125 ppb, Hayes et al., 2013). A range of ± 20 ppb uncertainty in background CO, results in an average ± 6 $\mu g\ m^{-3}\ ppm^{-1}$ uncertainty in OA/ΔCO. An increase in OA/ΔCO with aging is observed for ambient and reactor dark data (where reactor age = ambient photochemical age in the absence of internal reactor OH_{exp}), consistent with previous studies and as discussed in Hayes et al. (2013; 2015). The reactor data is consistent with SOA formation being dominated by shorter-lived precursors, as little increase in OA/ΔCO is observed after about a day of total age, consistent with the SIMPLE parameterization of urban SOA (Hodzic and Jimenez, 2011; Hayes et al., 2015).

To constrain the lifetimes of the important urban SOA precursors, the OH decays of three example gas-phase species (benzene, toluene, and 1,3,5-trimenthylbenzene (TMB)) are shown are overlaid in Fig. S10, together with data from Fig. 9 that illustrates the timescale over which OA/ΔCO increases. The correlation of different VOCs with maximum SOA formation in the reactor is shown vs. their reaction rate constants with OH (k_{OH}) in Figure 10. This analysis constrains the rate constants of the most important urban SOA precursors to the approximate k_{OH} ~ 3–5×10^{-11} cm^3 $molec^{-1}$ s^{-1}. This constraint suggests that polyalkyl monoaromatics (such as TMB), substituted polyaromatics such as alkyl naphthalenes (Phousongphouang and Arey, 2002), or large alkanes with ~23 or more carbons (Calvert et al., 2008), or branched / cyclic species of similar size are (as a group) important contributors. The latter species are semivolatile and intermediate volatility species (S/IVOCs), and thus our results suggests a very important role for such species in urban SOA formation. The timescale of SOA formation is in between those of TMB and toluene decays, mostly shorter than toluene decay and definitely shorter than benzene decay, again consistent with the previous discussion.

We note that in Fig. 9 aging of CO (decay of CO from reacting with OH in the reactor or atmosphere) was not included in the evolution of OA/ΔCO analysis, as the purpose of ΔCO is to serve as an inert tracer of the urban SOA precursors emitted into each airmass. However, when comparing with aged pollution observed in the field after e.g. a week of transport, the aging to the urban CO needs to be taken into account. This is shown in Fig. S10b, and indicates that ambient observations of very aged pollution would not show a decrease in OA/ΔCO due to photochemistry since the decreases in OA and CO at long photochemical ages have similar timescales. We note that a decrease in the OA/ΔCO ratio for ambient aged pollution may still be observed for other reasons such as wet deposition (Dunlea et al., 2009). Production of CO from urban VOCs is expected to be less than 1/10 of the directly emitted CO (Hallquist et al., 2009) and is neglected here.

4.2 Parameterization of the Amount and Timescale for Urban SOA Formation

The evolution of urban SOA vs. photochemical age follows a similar trend in different field studies with a rapid increase in the first day followed by a plateau at longer ages. Previously, this evolution has been fit with the SIMPLE parameterization, a 2-parameter model in which a single VOC precursor (VOC^*) is oxidized with a single rate constant with OH to produce non-volatile SOA. This parameterization has been shown to fit ambient data as well or better than more complex models (Hodzic and Jimenez, 2011; Hayes et al., 2015). However, the evolution of $OA/\Delta CO$ past the initial ~2 days is almost completely unconstrained by ambient observations, due to the difficulty of identifying urban pollution-dominated air masses after advection for several days, and of determining ΔCO when it is of the order of the uncertainties in the CO background. The reactor data from our study offer a unique opportunity to extend the model fit to much longer photochemical ages. The fit in Eqn. 1 was modified from Hayes et al. (2015)'s 2-parameter model for this purpose, where (POA+BGSOA)/CO is the primary OA plus background SOA, constrained at 16 $\mu g\ m^{-3}\ ppm^{-1}$ (Hayes et al., 2015), VOC^*/CO is the VOC^* emission ratio, and t is photochemical age, using measurements at local temperature and pressure.

$$\frac{OA}{\Delta CO} = \left\{\frac{POA + BGSOA}{CO} + \frac{VOC^*}{CO}\left[1 - e^{\left(\frac{-t}{\tau_1}\right)}\right]\right\} e^{\left(\frac{-t}{\tau_2}\right)} \qquad (1)$$

Fitting the reactor data in this way requires the addition of a 2nd timescale to account for loss of OA at long ages, as done in Eqn. 1. Fitting all ambient plus vapor loss-corrected data results in $VOC^*/CO = 56\pm5\ \mu g\ m^{-3}\ ppm^{-1}$, $\tau_1 = 0.3\pm0.1$ days, and $\tau_2 = 50\pm10$ days (Fig. 9, all data points, i.e. before averaged into quantiles is in Fig. S10a). In this parameterization, τ_1 is the timescale for urban SOA formation and τ_2 is the timescale for net OA mass loss due to fragmentation, likely dominated by heterogeneous oxidation. Kroll et al. (2015)'s laboratory examination of heterogeneous oxidation of OA found a volatilization lifetime of 70±20 days, supporting the 50±10 days timescales found in this work.

4.3 Comparison of Reactor output to Urban SOA Model Results

It is of interest to compare the SOA formation constrained from our reactor and ambient data to SOA models used in 3D modeling studies, as those models remain poorly constrained (e.g. Hayes et al., 2015). Here we used two of the model variants recently described in Hayes et al. (2015), and compare to our data in Fig. 11. The first model variant is a "traditional model" with SOA formation from VOCs using pre-2007 yields (Koo et al., 2003), which has been shown before to underpredict urban SOA formation by over an order-of-magnitude (Dzepina et al., 2009; Morino et al., 2014; Hayes et al., 2015). This comparison is still of interest as several SOA models still use this approach (e.g. Morino et al., 2014; Baker et al., 2015; Hayes et al., 2015).

The second model variant represents SOA formation semivolatile and intermediate volatility precursors (P-S/IVOC; Robinson et al., 2007) in addition to VOCs, and has been shown to predict SOA formation adequately at short timescales (<1 day) but to overpredict at long ages (Dzepina et al., 2011; Hayes et al., 2015). SOA formation from VOCs uses the Tsimpidi et al. (2010) formulation, including "aging" of the SOA, and using the high NO_x yields since the observed SOA formation mostly occurs in the urban environment where RO_2 react mainly with NO (Hayes et al., 2015). SOA from P-S/IVOCs is represented using the Robinson et al. (2007) parameterization. Recent results suggest that P-S/IVOC are needed to explain SOA formation observed in ambient air during CalNex (Zhao et al., 2014; Hayes et al., 2015), consistent with other locations (Dzepina et al., 2009; Hodzic et al., 2010).

Figure 11a shows the comparison of the SOA models against our ambient and reactor results. The traditional model predicts SOA a factor of 10 lower than our observations, consistent with previous studies. The updated model performance is mixed: the magnitude of SOA formation at short times (<1 day) is somewhat slower but similar to the ambient data. SOA formation at long ages (>1 day) is significantly overpredicted by a factor of ~3. This model does not include heterogeneous oxidation reactions leading to fragmentation which could decrease predicted OA at high photochemical ages, resulting in a wider discrepancy at very long ages (>10 days). Figure 11b shows the same comparison using lower IVOCs as suggested from field measurements (Zhao et al., 2014). The same model was used, but with the initial concentrations of primary IVOCs decreased by one-half to better match the ambient observations of Zhao et al. (2014), as described by Hayes et al. (2015). This difference is due to the different methods used to estimate the background SOA. Briefly, in this work as well as in Hayes et al. (2015), the background SOA is estimated to be equal to the minimum low-volatility oxygenated organic aerosol (LV-OOA) concentration in the diurnal cycle. Whereas in Hayes et al. (2013), the background SOA was estimated to be equal to the mean LV-OOA concentration for photochemical ages less than 1.2 h. Decreasing IVOCs brings down overall SOA predictions, increasing the discrepancy at shorter ages and still overestimating SOA concentrations compared to reactor measurements at the longest ages. This result suggests that the reduced IVOC concentrations cannot account for all model discrepancies. It is of interest to compare the reactor results with those of other SOA mechanisms in the future.

4.4 Evolution at High Photochemical Ages

The photochemical evolution of OA at long ages is of high interest as it partially controls the background of OA at remote locations where it may influence climate more strongly, due to the higher sensitivity of clouds to aerosols at low aerosol concentrations (Reutter et al., 2009). Heald et al. (2011) noted that a process that consumed OA with a timescale of ~10 days was needed in order to avoid overpredictions of OA in remote air. Heterogeneous oxidation is thought to play an important role for long photochemical ages, while being too slow to compete at timescales of a day or so (DeCarlo et al., 2008; George and Abbatt, 2010). Fig. 12a compares our CalNex results to heterogeneous OH oxidation of ambient air from George and Abbatt (2010) using a similar oxidation flow reactor (Toronto Photo-Oxidation Tube, TPOT), but with gas-phase SOA precursors removed by a denuder. Note that no SOA formation is observed for the George and Abbatt case due to the use of a denuder, and thus only the data for $ER_{OA} < 1$ can be approximately compared. The two datasets show a similar trend with the start of a net decrease around 2 weeks of oxidation and a similar evolution. A decrease in SOA yields at high ages (>7 days) was also observed by Lambe et al. (2012), in experiments where SOA was formed from gaseous precursors. Note that the George and Abbatt (2010) vs. Lambe et al. (2012) studies are qualitatively different, and thus the explanations of the decrease in OA at high ages may be different. George and Abbatt (2010) started their oxidation experiment with particles only, after removing gases with a denuder. Any decreases in OA in their study must result from heterogeneous oxidation. The Lambe et al. (2012) study started with gas-phase precursors only and no particles. Thus the reduction in SOA at high OH_{exp} may be due to either gas-phase fragmentation of condensable species, so that SOA is never formed, or to formation of SOA followed by its heterogeneous oxidation and revolatilization. Results in Fig. S7 suggest that gas-phase oxidation would prevent the formation of SOA, and thus the second explanation is more likely.

To evaluate directly whether heterogeneous oxidation could explain the gain of oxygen observed in the aerosol, we follow the method outlined in appendix A of DeCarlo et al. (2008). Fig. S11 shows the ratio of the gain of oxygen of OA observed in the reactor (ΔOxygen in OA = $O_{\text{atoms, reactor}} - O_{\text{atoms, ambient}}$) to the total number of OH collisions with OA in the reactor, plotted vs. total photochemical age. Heterogeneous oxidation calculations use surface-weighted diameter calculated from the peak of the mass distribution and estimated particle density from AMS components (DeCarlo et al., 2004), assume every collision results in reaction ($\gamma = 1$). If it is assumed that each OH collision with OA results in one O atom addition, the number of O atoms added is underpredicted by a factor of 5 at ages ∼ 1 day, decreasing to a factor of 2 at ∼ 10 days, and lower values at high ages (> 10 days). This analysis supports that heterogeneous oxidation is not dominant in contributing to SOA mass at low-to-intermediate ages, but it likely plays a role in OA evolution at the highest photochemical ages in the reactor.

An alternative explanation for the loss of OA at high photochemical ages is that the reaction of semivolatile gas species with OH (leading to fragmentation and thus non-condensing species) can lead to OA evaporation as the semivolatile species in the particles evaporate to re-establish equilibrium partitioning. However, most of OA has too low volatility to evaporate in response to the removal of semivolatile species from the gas phase. Fig. S12 shows the volatility distribution estimated for CalNex OA using concurrent thermal denuder measurements (Huffman et al., 2008; Faulhaber et al., 2009). As observed in other locations (Cappa and Jimenez, 2010), only ~20% of the OA is susceptible of evaporation upon removal of the gas phase. Losing ~60% of the OA would be the equivalent of heating to 100˚C in a thermal denuder. Thus, there is not enough semivolatile material available to account for that degree of loss observed in our reactor measurements. We note that some models predict SOA that is too volatile (Dzepina et al., 2009), and if applied in a flow reactor context they may wrongly predict a large effect from semivolatile evaporation. Additionally, timescales for ambient OA evaporation upon removal of gas-phase organics from field measurements has been shown to be slow and size dependent, with fast evaporation up to only ~20% of OA mass happening on the order of ~100 min, followed by much slower evaporation of the order of days (Vaden et al., 2011). Given the short residence time utilized in the reactor during this study (< 5 minutes), there is not significant time to allow for substantial repartitioning of OA in equilibrium with semivolatile gas-phase organics.

4.5 Comparison to a recent Reactor Study in a Tunnel

It is of interest to compare the evolution of urban SOA vs. photochemical age determined in this work with a recently published study with a similar flow reactor in a vehicle tunnel in Pittsburgh, PA (Tkacik et al., 2014). Whether urban SOA is formed predominantly from vehicle emissions has been the subject of recent debate (Ensberg et al., 2014). The data are compared in Fig. 12b as SOA/ΔCO, where ambient POA and background OA have been subtracted from our reactor data to compare to Tkacik et al. (2014)'s SOA-only measurement. Since the tunnel data has not been corrected for vapor losses in the reactor, we only show uncorrected CalNex reactor data for this comparison.

The tunnel experiment shows qualitatively similar results, with an initial increase to a peak of the same order, followed by a decrease in SOA/ΔCO at high ages. The initial SOA rise and peak occur at higher OH_{exp} than observed in CalNex ambient data and in previous ambient urban studies, as well as our flow reactor data. The difference at low ages between the tunnel and the other studies may be due to several reasons:

(1) Possible OH_{exp} overestimation in the tunnel study. OH_{exp} in flow reactors can be reduced by 1-2 orders of magnitude by high levels of OH reactivity from high concentrations of very fresh emissions, such as those present in the tunnel environment (Li et al., 2015; Peng et al., 2015). OH_{exp} was corrected for OH suppression in the tunnel study using laboratory experiments with NO levels similar to the tunnel. However, the OH reactivity of NO_x is expected to decay much faster than that of VOCs and their reaction products. Thus the OH suppression in the tunnel study was likely underestimated (Peng et al., 2015) as OH suppression from VOCs was not considered. Since OH suppression is largest at low OH_{exp} that effect may account for the deviation observed at low ages while having a much smaller effect on the tunnel data at high ages.

(2) There may be substantial losses of semivolatiles in the inlet of the tunnel study. In contrast, our flow reactor was operated without an inlet to minimize the loss of semivolatiles, based on an observation in a previous study of a substantial reduction in SOA formation when any inlet or an inlet plate was used (Ortega et al., 2013). Since semivolatile primary species are larger molecules with faster OH rate constants (Ziemann and Atkinson, 2012), that could explain the lack of SOA formation at ages below a day, compared to the large amount of SOA formed for those ages in the ambient CalNex observations (Hayes et al., 2013; 2015). However the fact that the magnitude of eventual SOA formation is larger in the tunnel study argues against this possibility.

(3) It may appear at first that the tunnel SOA may have have been dominated by RO_2+NO, compared to RO_2+HO_2 for our ambient air results, thus making the results less comparable. However, while the initial NO levels in the tunnel may be high, the lifetime of NO under the conditions of the OFR is typically very low (Li et al., 2015). O_3 levels in OFR185 are typically 1–25 ppm, which result in NO lifetimes of 0.1–2 s. Since HO_2 levels are greatly enhanced by the reactor chemistry, the majority of the RO_2 radicals are still expected to react via RO_2 + HO_2 under

the tunnel conditions, similar to our study. The model of Peng et al. (2015) was used to estimate the fraction of RO_2 reacting with NO vs. HO_2 for the tunnel study. At the point of peak SOA production we estimate that 81% of the RO_2 radicals are reacting with HO_2 and 19% with NO. Therefore the chemistry of the OFR in the tunnel study is proceeding mostly through the HO_2 channel, similar to our ambient study.

(4) A difference between the studies that may explain somewhat higher SOA formation in the tunnel study is the larger partitioning of semivolatile species, given the higher OA concentrations (~50 $\mu g\ m^{-3}$ in the tunnel vs ~15 $\mu g\ m^{-3}$ for our study). However this effect is estimated to be a factor of ~1.5 for the aromatic and alkane precursors that are thought to dominate SOA formation from vehicle emissions (Barsanti et al., 2013), and it reduces the difference observed here, thus further supporting our conclusions.

Thus it is most likely that the observed difference between the tunnel and our study is due to overestimation of OH_{exp} at lower ages in the tunnel study. We have used the model of Peng et al. (2015) to estimate the corrected OH_{exp} under the tunnel conditions. The corrected curve is also shown in Fig. 12b, and shows much improved agreement with our urban air observations.

A recent study examining the ambient SOA results from CalNex concluded that either vehicle emissions are not the dominant source of SOA in the LA Basin, or that the ambient SOA mass yields are much larger than what has been derived experimentally (Ensberg et al., 2014). Given the similar magnitude and timing (after correction for OH suppression) of SOA formation in the tunnel vs. ambient data and the fact that most urban CO arises from motor vehicles, the combination of both studies strongly suggests that motor vehicles are the dominant source of urban SOA, and that the SOA yields from vehicle emissions are much larger than estimated from measured VOCs as by Ensberg et al. (2014). The contribution of typically unmeasured S/IVOCs to SOA may explain the missing vehicle SOA, as discussed in section 4.3.

5 Summary and Conclusions

Real-time measurement of SOA formation and OA aging was carried out with a photochemical oxidation flow reactor coupled to an AMS and SMPS during the CalNex field campaign and targeted urban emissions. This work represents the first applications of an oxidation flow reactor to investigate SOA formation from ambient urban air, to our knowledge. Continuous ambient air sampling through the reactor provides complementary information to the analysis of ambient data at the site, and provides constraints on the evolution of urban SOA at long ages that are very difficult to observe with ambient measurements. Additionally, these uninterrupted reactor measurements over a two-week period allowed for observations over a prolonged period of stagnant air accumulating urban emissions.

OA enhancement peaked between 0.8–6 days of atmospheric equivalent aging (OH_{exp} = 1.0–5.2×10^{11} molec. cm^{-3} s). Reactor OA mass showed net destruction decreasing below ambient concentrations after two weeks of atmospheric equivalent aging (OH_{exp} above 2×10^{12} molec. cm^{-3} s) suggesting a shift from chemistry dominated by functionalization/condensation to one dominated by heterogeneous oxidation leading to fragmentation/evaporation, but with functionalization still occurring. Comparison to reactor experiments of heterogeneous oxidation of ambient air shows similar trends to those observed for high ages in this study. High OA enhancement was observed at night (ER_{OA} ~2, delta OA ~5μg/m^3) with reactor-aged OA mass peaking at concentrations similar to peak daytime ambient OA mass. Reactor-derived OA mass enhancement correlates with 1,3,5-trimethylbenzene, and has an inverse relationship with O_x and ambient OOA, suggesting that short-lived precursors (τ_{OH} ~ few hours) dominate SOA formation in the LA-Basin.

The chemical evolution of OA in the reactor was examined with a Van Krevelen diagram (H:C vs. O:C). Reactor-aged OA produces a similar slope (~ -0.65) to that observed in ambient OA, thus is consistent with the reactor producing similar functionalization to ambient oxidation. While total OA mass was observed to decrease at very high OH exposures, O:C continued to increase. Oxidation state of carbon peaked at high values (OS_C ~2 at highest OH_{exp}), similar to ambient observations of low volatility OA.

Modeling results indicate predicted maximum SOA from traditional models is a factor of 10 less than the maximum OA mass enhancement observed from aging ambient air in the reactor, consistent with previous comparisons using ambient data. Updated VBS-based models including both VOC and S/IVOC overpredict SOA formation by a factor of 2–3 at intermediate to high ages. If the IVOC emissions are reduced by a factor of 2 in the updated model to fit recent CalNex observations, the discrepancy between model and observation is reduced but these models cannot capture the reduction of SOA mass concentration that is observed with the OFR at longer OH exposures.

Evolution of the ratio of OA/ΔCO vs. photochemical age shows the reactor produces results consistent with the ambient data. At ages beyond those reliably observed for ambient OA, the reactor observations show a leveling and then decrease in OA/ΔCO. A fit of this data results in a timescale of SOA formation ~0.3 days and fragmentation-dominated heterogeneous oxidation and net mass loss with a timescale of ~50 days. The fit derived in this work may be useful in future studies, e.g. as a check on proposed model-parameterizations of urban SOA formation.

Comparison to a similar reactor experiment aging vehicular emissions in a tunnel shows consistent results with our study, once a likely overestimation of OH_{exp} at low ages in the tunnel is taken into account. The combination of both studies strongly suggests that vehicle emissions do dominate urban SOA formation and their SOA formation potential is higher than when only VOCs are considered.

This study shows that oxidation flow reactors are useful tools as part of ambient field studies, as they allow real-time measurement of SOA formation potential and oxidation across a wide range of photochemical ages. These results help constrain SOA models not only for the growth phase of the SOA but also for the decay phase, when further aging removes SOA mass. Future studies should apply this technique in other cities and other environments such as forested regions and the outflow from polluted continents, in order to further constrain the SOA formation potential and timescales for different sources and regions.

Acknowledgements

We thank CARB 08-319 and 11-305, DOE (BER, ASP Program) DE-SC0006035 and DE-SC0011105, NOAA NA13OAR4310063, and NSF AGS-1243354 and AGS-1360834 for partial support of this work. AMO and PLH acknowledge fellowships from the DOE SCGP Fellowship Program (ORAU, ORISE) and the CIRES Visiting Fellowship program, respectively. WHB acknowledges the support by NSF (grant ATM-0919079). We thank Phil Stevens' research group (Indiana University) for use of OH reactivity data from the CalNex Pasadena ground site. We are grateful to Jochen Stutz (UCLA), John Seinfeld (Caltech), and Jason Surratt (UNC-Chapel Hill) for co-organization of the CalNex Supersite, and to CARB for supporting the infrastructure at the site. We also thank John S. Holloway (NOAA) for providing CO data, Roya Bahreini (University of California-Riverside), and Ann M. Middlebrook (NOAA) for providing OA data from the NOAA WP-3D. We thank Carlos Martinez (Univ. Jaen) for useful discussions about CFD modeling of the OFR.

References

Aiken, A. C., DeCarlo, P. F., Kroll, J. H., Worsnop, D. R., Huffman, J. A., Docherty, K. S., Ulbrich, I. M., Mohr, C., Kimmel, J. R., Sueper, D., Sun, Y., Zhang, Q., Trimborn, A., Northway, M., Ziemann, P. J., Canagaratna, M. R., Onasch, T. B., Alfarra, M. R., Prevot, A. S. H., Dommen, J., Duplissy, J., Metzger, A., Baltensperger, U., and Jimenez, J. L.: O/C and OM/OC Ratios of Primary, Secondary, and Ambient Organic Aerosols with High-Resolution Time-of-Flight Aerosol Mass Spectrometry, Environmental Science & Technology, 42, 4478-4485, 10.1021/es703009q, 2008.

Atkinson, R., Baulch, D. L., Cox, R. A., Crowley, J. N., Hampson, R. F., Hynes, R. G., Jenkin, M. E., Rossi, M. J., Troe, J., and Subcommittee, I.: Evaluated kinetic and photochemical data for atmospheric chemistry: Volume II: gas phase reactions of organic species, Atmos. Chem. Phys., 6, 3625-4055, 10.5194/acp-6-3625-2006, 2006.

Bahreini, R., Middlebrook, A. M., Brock, C. A., de Gouw, J. A., McKeen, S. A., Williams, L. R., Daumit, K. E., Lambe, A. T., Massoli, P., Canagaratna, M. R., Ahmadov, R., Carrasquillo, A. J., Cross, E. S., Ervens, B., Holloway, J. S., Hunter, J. F., Onasch, T. B., Pollack, I. B., Roberts, J. M., Ryerson, T. B., Warneke, C., Davidovits, P., Worsnop, D. R., and Kroll, J. H.: Mass Spectral Analysis of Organic Aerosol Formed Downwind of the Deepwater Horizon Oil Spill: Field Studies and Laboratory Confirmations, Environmental Science & Technology, 46, 8025-8034, 10.1021/es301691k, 2012a.

Bahreini, R., Middlebrook, A. M., de Gouw, J. A., Warneke, C., Trainer, M., Brock, C. A., Stark, H., Brown, S. S., Dube, W. P., Gilman, J. B., Hall, K., Holloway, J. S., Kuster, W. C., Perring, A. E., Prevot, A. S. H., Schwarz, J. P., Spackman, J. R., Szidat, S., Wagner, N. L., Weber, R. J., Zotter, P., and Parrish, D. D.: Gasoline emissions dominate over diesel in formation of secondary organic aerosol mass, Geophysical Research Letters, 39, 10.1029/2011gl050718, 2012b.

Baker, K. R., Carlton, A. G., Kleindienst, T. E., Offenberg, J. H., Beaver, M. R., Gentner, D. R., Goldstein, A. H., Hayes, P. L., Jimenez, J. L., Gilman, J. B., de Gouw, J. A., Woody, M. C., Pye, H. O. T., Kelly, J. T., Lewandowski, M., Jaoui, M., Stevens, P. S., Brune, W. H., Lin, Y. H., Rubitschun, C. L., and Surratt, J. D.: Gas and aerosol carbon in California: comparison of measurements and model predictions in Pasadena and Bakersfield, Atmos. Chem. Phys., 15, 5243-5258, 10.5194/acp-15-5243-2015, 2015.

Barsanti, K. C., Carlton, A. G., and Chung, S. H.: Analyzing experimental data and model parameters: implications for predictions of SOA using chemical transport models, Atmos. Chem. Phys., 13, 12073-12088, 10.5194/acp-13-12073-2013, 2013.

Borbon, A., Gilman, J. B., Kuster, W. C., Grand, N., Chevaillier, S., Colomb, A., Dolgorouky, C., Gros, V., Lopez, M., Sarda-Esteve, R., Holloway, J., Stutz, J., Petetin, H., McKeen, S., Beekmann, M., Warneke, C., Parrish, D. D., and de Gouw, J. A.: Emission ratios of anthropogenic volatile organic compounds in northern mid-latitude megacities: Observations versus emission inventories in Los Angeles and Paris, Journal of Geophysical Research: Atmospheres, 118, 2041-2057, 10.1002/jgrd.50059, 2013.

Bruns, E. A., El Haddad, I., Keller, A., Klein, F., Kumar, N. K., Pieber, S. M., Corbin, J. C., Slowik, J. G., Brune, W. H., Baltensperger, U., and Prévôt, A. S. H.: Inter-comparison of laboratory smog chamber and flow reactor systems on organic aerosol yield and composition, Atmos. Meas. Tech. Discuss., 8, 309-352, 10.5194/amtd-8-309-2015, 2015.

Calvert, J. G., Derwent, R. G., Orlando, J. J., Tyndall, G. S., and Wallington, T. J.: Mechanisms of Atmospheric Oxidation of the Alkanes, Oxford University Press, 2008.

Canagaratna, M. R., Jayne, J. T., Jimenez, J. L., Allan, J. D., Alfarra, M. R., Zhang, Q., Onasch, T. B., Drewnick, F., Coe, H., Middlebrook, A., Delia, A., Williams, L. R., Trimborn, A. M., Northway, M. J., DeCarlo, P. F., Kolb, C. E., Davidovits, P., and Worsnop, D. R.: Chemical and microphysical characterization of ambient aerosols with the aerodyne aerosol mass spectrometer, Mass Spectrom Rev, 26, 185-222, Doi 10.1002/Mas.20115, 2007.

Canagaratna, M. R., Jimenez, J. L., Kroll, J. H., Chen, Q., Kessler, S. H., Massoli, P., Hildebrandt Ruiz, L., Fortner, E., Williams, L. R., Wilson, K. R., Surratt, J. D., Donahue, N. M., Jayne, J. T., and Worsnop, D. R.: Elemental ratio measurements of organic compounds using aerosol mass spectrometry: characterization, improved calibration, and implications, Atmos. Chem. Phys., 15, 253-272, 10.5194/acp-15-253-2015, 2015.

Cao, G., and Jang, M.: Effects of particle acidity and UV light on secondary organic aerosol formation from oxidation of aromatics in the absence of NOx, Atmospheric Environment, 41, 7603-7613, http://dx.doi.org/10.1016/j.atmosenv.2007.05.034, 2007.

Cappa, C. D., and Jimenez, J. L.: Quantitative estimates of the volatility of ambient organic aerosol, Atmos. Chem. Phys., 10, 5409-5424, 10.5194/acp-10-5409-2010, 2010.

Cubison, M. J., Ortega, A. M., Hayes, P. L., Farmer, D. K., Day, D., Lechner, M. J., Brune, W. H., Apel, E., Diskin, G. S., Fisher, J. A., Fuelberg, H. E., Hecobian, A., Knapp, D. J., Mikoviny, T., Riemer, D., Sachse, G. W., Sessions, W., Weber, R. J., Weinheimer, A. J., Wisthaler, A., and Jimenez, J. L.: Effects of aging on organic aerosol from open biomass burning smoke in aircraft and laboratory studies, Atmos Chem Phys, 11, 12049-12064, 2011.

de Gouw, J., and Jimenez, J. L.: Organic Aerosols in the Earth's Atmosphere, Environmental Science & Technology, 43, 7614-7618, 10.1021/es9006004, 2009.

de Gouw, J. A., Middlebrook, A. M., Warneke, C., Goldan, P. D., Kuster, W. C., Roberts, J. M., Fehsenfeld, F. C., Worsnop, D. R., Canagaratna, M. R., Pszenny, A. A. P., Keene, W. C., Marchewka, M., Bertman, S. B., and Bates, T. S.: Budget of organic carbon in a polluted atmosphere: Results from the New England Air Quality Study in 2002, J. Geophys. Res., 110, D16305, 10.1029/2004jd005623, 2005.

DeCarlo, P. F., Slowik, J. G., Worsnop, D. R., Davidovits, P., and Jimenez, J. L.: Particle morphology and density characterization by combined mobility and aerodynamic diameter measurements. Part 1: Theory, Aerosol Sci Tech, 38, 1185-1205, 2004.

DeCarlo, P. F., Kimmel, J. R., Trimborn, A., Northway, M. J., Jayne, J. T., Aiken, A. C., Gonin, M., Fuhrer, K., Horvath, T., Docherty, K., Worsnop, D. R., and Jimenez, J. L.: Field-Deployable, High-Resolution, Time-of-Flight Aerosol Mass Spectrometer, Analytical Chemistry, 78, 8281-8289, 2006.

DeCarlo, P. F., Dunlea, E. J., Kimmel, J. R., Aiken, A. C., Sueper, D., Crounse, J., Wennberg, P. O., Emmons, L., Shinozuka, Y., Clarke, A., Zhou, J., Tomlinson, J., Collins, D. R., Knapp, D., Weinheimer, A. J., Montzka, D. D., Campos, T., and Jimenez, J. L.: Fast airborne aerosol size and chemistry measurements above Mexico City and Central Mexico during the MILAGRO campaign, Atmos. Chem. Phys., 8, 4027-4048, 10.5194/acp-8-4027-2008, 2008.

DeCarlo, P. F., Ulbrich, I. M., Crounse, J., de Foy, B., Dunlea, E. J., Aiken, A. C., Knapp, D., Weinheimer, A. J., Campos, T., Wennberg, P. O., and Jimenez, J. L.: Investigation of the sources and processing of organic aerosol over the Central Mexican Plateau from aircraft measurements during MILAGRO, Atmos. Chem. Phys., 10, 5257-5280, 10.5194/acp-10-5257-2010, 2010.

Docherty, K. S., Stone, E. A., Ulbrich, I. M., DeCarlo, P. F., Snyder, D. C., Schauer, J. J., Peltier, R. E., Weber, R. J., Murphy, S. M., Seinfeld, J. H., Grover, B. D., Eatough, D. J., and Jimenez, J. L.: Apportionment of Primary and Secondary Organic Aerosols in Southern California during the 2005 Study of Organic Aerosols in Riverside (SOAR-1), Environmental Science & Technology, 42, 7655-7662, 10.1021/es8008166, 2008.

Docherty, K. S., Aiken, A. C., Huffman, J. A., Ulbrich, I. M., DeCarlo, P. F., Sueper, D., Worsnop, D. R., Snyder, D. C., Peltier, R. E., Weber, R. J., Grover, B. D., Eatough, D. J., Williams, B. J., Goldstein, A. H., Ziemann, P. J., and Jimenez, J. L.: The 2005 Study of Organic Aerosols at Riverside (SOAR-1): instrumental intercomparisons and fine particle composition, Atmos. Chem. Phys., 11, 12387-12420, 10.5194/acp-11-12387-2011, 2011.

Donahue, N. M., Robinson, A. L., Stanier, C. O., and Pandis, S. N.: Coupled Partitioning, Dilution, and Chemical Aging of Semivolatile Organics, Environmental Science & Technology, 40, 2635-2643, 10.1021/es052297c, 2006.

Donahue, N. M., Chuang, W., Epstein, S. A., Kroll, J. H., Worsnop, D. R., Robinson, A. L., Adams, P. J., and Pandis, S. N.: Why do organic aerosols exist? Understanding aerosol lifetimes using the two-dimensional volatility basis set, Environ Chem, 10, 151-157, Doi 10.1071/En13022, 2013.

Drewnick, F., Hings, S. S., DeCarlo, P., Jayne, J. T., Gonin, M., Fuhrer, K., Weimer, S., Jimenez, J. L., Demerjian, K. L., Borrmann, S., and Worsnop, D. R.: A New Time-of-Flight Aerosol Mass Spectrometer (TOF-AMS)—Instrument Description and First Field Deployment, Aerosol Science and Technology, 39, 637-658, 10.1080/02786820500182040, 2005.

Dunlea, E. J., DeCarlo, P. F., Aiken, A. C., Kimmel, J. R., Peltier, R. E., Weber, R. J., Tomlinson, J., Collins, D. R., Shinozuka, Y., McNaughton, C. S., Howell, S. G., Clarke, A. D., Emmons, L. K., Apel, E. C., Pfister, G. G., van Donkelaar, A., Martin, R. V., Millet, D. B., Heald, C. L., and Jimenez, J. L.: Evolution of Asian aerosols during transpacific transport in INTEX-B, Atmos. Chem. Phys., 9, 7257-7287, 10.5194/acp-9-7257-2009, 2009.

Dzepina, K., Volkamer, R. M., Madronich, S., Tulet, P., Ulbrich, I. M., Zhang, Q., Cappa, C. D., Ziemann, P. J., and Jimenez, J. L.: Evaluation of recently-proposed secondary organic aerosol models for a case study in Mexico City, Atmos. Chem. Phys., 9, 5681-5709, 10.5194/acp-9-5681-2009, 2009.

Dzepina, K., Cappa, C. D., Volkamer, R. M., Madronich, S., DeCarlo, P. F., Zaveri, R. A., and Jimenez, J. L.: Modeling the Multiday Evolution and Aging of Secondary Organic Aerosol During MILAGRO 2006, Environmental Science & Technology, 45, 3496-3503, 10.1021/es103186f, 2011.

Ensberg, J. J., Hayes, P. L., Jimenez, J. L., Gilman, J. B., Kuster, W. C., de Gouw, J. A., Holloway, J. S., Gordon, T. D., Jathar, S., Robinson, A. L., and Seinfeld, J. H.: Emission factor ratios, SOA mass yields, and the impact of vehicular emissions on SOA formation, Atmos. Chem. Phys., 14, 2383-2397, 10.5194/acp-14-2383-2014, 2014.

Ervens, B., Turpin, B. J., and Weber, R. J.: Secondary organic aerosol formation in cloud droplets and aqueous particles (aqSOA): a review of laboratory, field and model studies, Atmos. Chem. Phys., 11, 11069-11102, 10.5194/acp-11-11069-2011, 2011.

Faulhaber, A. E., Thomas, B. M., Jimenez, J. L., Jayne, J. T., Worsnop, D. R., and Ziemann, P. J.: Characterization of a thermodenuder-particle beam mass spectrometer system for the study of organic aerosol volatility and composition, Atmos. Meas. Tech., 2, 15-31, 10.5194/amt-2-15-2009, 2009.

George, I. J., and Abbatt, J. P. D.: Heterogeneous oxidation of atmospheric aerosol particles by gas-phase radicals, Nat Chem, 2, 713-722, 2010.

Hallquist, M., Wenger, J. C., Baltensperger, U., Rudich, Y., Simpson, D., Claeys, M., Dommen, J., Donahue, N. M., George, C., Goldstein, A. H., Hamilton, J. F., Herrmann, H., Hoffmann, T., Iinuma, Y., Jang, M., Jenkin, M. E., Jimenez, J. L., Kiendler-Scharr, A., Maenhaut, W., McFiggans, G., Mentel, T. F., Monod, A., Prévôt, A. S. H., Seinfeld, J. H., Surratt, J. D., Szmigielski, R., and Wildt, J.: The formation, properties and impact of secondary organic aerosol: current and emerging issues, Atmos. Chem. Phys., 9, 5155-5236, 10.5194/acp-9-5155-2009, 2009.

Hayes, P. L., Ortega, A. M., Cubison, M. J., Froyd, K. D., Zhao, Y., Cliff, S. S., Hu, W. W., Toohey, D. W., Flynn, J. H., Lefer, B. L., Grossberg, N., Alvarez, S., Rappenglück, B., Taylor, J. W., Allan, J. D., Holloway, J. S., Gilman, J. B., Kuster, W. C., de Gouw, J. A., Massoli, P., Zhang, X., Liu, J., Weber, R. J., Corrigan, A. L., Russell, L. M., Isaacman, G., Worton, D. R., Kreisberg, N. M., Goldstein, A. H., Thalman, R., Waxman, E. M., Volkamer, R., Lin, Y. H., Surratt, J. D., Kleindienst, T. E., Offenberg, J. H., Dusanter, S., Griffith, S., Stevens, P. S., Brioude, J., Angevine, W. M., and Jimenez, J. L.: Organic aerosol composition and sources in Pasadena, California, during the 2010 CalNex campaign, Journal of Geophysical Research: Atmospheres, 118, 9233-9257, 10.1002/jgrd.50530, 2013.

Hayes, P. L., Carlton, A. G., Baker, K. R., Ahmadov, R., Washenfelder, R. A., Alvarez, S., Rappenglück, B., Gilman, J. B., Kuster, W. C., de Gouw, J. A., Zotter, P., Prévôt, A. S. H., Szidat, S., Kleindienst, T. E., Offenberg, J. H., Ma, P. K., and Jimenez, J. L.: Modeling the formation and aging of secondary organic aerosols in Los Angeles during CalNex 2010, Atmos. Chem. Phys., 15, 5773-5801, 10.5194/acp-15-5773-2015, 2015.

Heald, C. L., Kroll, J. H., Jimenez, J. L., Docherty, K. S., DeCarlo, P. F., Aiken, A. C., Chen, Q., Martin, S. T., Farmer, D. K., and Artaxo, P.: A simplified description of the evolution of organic aerosol composition in the atmosphere, Geophys. Res. Lett., 37, L08803, 10.1029/2010gl042737, 2010.

Heald, C. L., Coe, H., Jimenez, J. L., Weber, R. J., Bahreini, R., Middlebrook, A. M., Russell, L. M., Jolleys, M., Fu, T. M., Allan, J. D., Bower, K. N., Capes, G., Crosier, J., Morgan, W. T., Robinson, N. H., Williams, P. I., Cubison, M. J., DeCarlo, P. F., and Dunlea, E. J.: Exploring the vertical profile of atmospheric organic aerosol: comparing 17 aircraft field campaigns with a global model, Atmos. Chem. Phys., 11, 12673-12696, 10.5194/acp-11-12673-2011, 2011.

Herndon, S. C., Onasch, T. B., Wood, E. C., Kroll, J. H., Canagaratna, M. R., Jayne, J. T., Zavala, M. A., Knighton, W. B., Mazzoleni, C., Dubey, M. K., Ulbrich, I. M., Jimenez, J. L., Seila, R., de Gouw, J. A., de Foy, B., Fast, J., Molina, L. T., Kolb, C. E., and Worsnop, D. R.: Correlation of secondary organic aerosol with odd oxygen in Mexico City, Geophysical Research Letters, 35, L15804, 10.1029/2008gl034058, 2008.

Hersey, S. P., Craven, J. S., Schilling, K. A., Metcalf, A. R., Sorooshian, A., Chan, M. N., Flagan, R. C., and Seinfeld, J. H.: The Pasadena Aerosol Characterization Observatory (PACO): chemical and physical analysis of the Western Los Angeles basin aerosol, Atmos. Chem. Phys., 11, 7417-7443, 10.5194/acp-11-7417-2011, 2011.

Hodzic, A., Jimenez, J. L., Madronich, S., Canagaratna, M. R., DeCarlo, P. F., Kleinman, L., and Fast, J.: Modeling organic aerosols in a megacity: potential contribution of semi-volatile and intermediate volatility primary organic compounds to secondary organic aerosol formation, Atmos. Chem. Phys., 10, 5491-5514, 10.5194/acp-10-5491-2010, 2010.

Hodzic, A., and Jimenez, J. L.: Modeling anthropogenically controlled secondary organic aerosols in a megacity: a simplified framework for global and climate models, Geosci. Model Dev., 4, 901-917, 10.5194/gmd-4-901-2011, 2011.

Huffman, J. A., Ziemann, P. J., Jayne, J. T., Worsnop, D. R., and Jimenez, J. L.: Development and Characterization of a Fast-Stepping/Scanning Thermodenuder for Chemically-Resolved Aerosol Volatility Measurements, Aerosol Science and Technology, 42, 395-407, 10.1080/02786820802104981, 2008.

Huffman, J. A., Docherty, K. S., Aiken, A. C., Cubison, M. J., Ulbrich, I. M., DeCarlo, P. F., Sueper, D., Jayne, J. T., Worsnop, D. R., Ziemann, P. J., and Jimenez, J. L.: Chemically-resolved aerosol volatility measurements from two megacity field studies, Atmos Chem Phys, 9, 7161-7182, 2009.

Jimenez, J. L., Canagaratna, M. R., Donahue, N. M., Prevot, A. S. H., Zhang, Q., Kroll, J. H., DeCarlo, P. F., Allan, J. D., Coe, H., Ng, N. L., Aiken, A. C., Docherty, K. S., Ulbrich, I. M., Grieshop, A. P., Robinson, A. L., Duplissy, J., Smith, J. D., Wilson, K. R., Lanz, V. A., Hueglin, C., Sun, Y. L., Tian, J., Laaksonen, A., Raatikainen, T., Rautiainen, J., Vaattovaara, P., Ehn, M., Kulmala, M., Tomlinson, J. M., Collins, D. R., Cubison, M. J., Dunlea, E. J., Huffman, J. A., Onasch, T. B., Alfarra, M. R., Williams, P. I., Bower, K., Kondo, Y., Schneider, J., Drewnick, F., Borrmann, S., Weimer, S., Demerjian, K., Salcedo, D., Cottrell, L., Griffin, R., Takami, A., Miyoshi, T., Hatakeyama, S., Shimono, A., Sun, J. Y., Zhang, Y. M., Dzepina, K., Kimmel, J. R., Sueper, D., Jayne, J. T., Herndon, S. C., Trimborn, A. M., Williams, L. R., Wood, E. C., Middlebrook, A. M., Kolb, C. E., Baltensperger, U., and Worsnop, D. R.: Evolution of Organic Aerosols in the Atmosphere, Science, 326, 1525-1529, 2009.

Kang, E., Root, M. J., Toohey, D. W., and Brune, W. H.: Introducing the concept of Potential Aerosol Mass (PAM), Atmos. Chem. Phys., 7, 5727-5744, 10.5194/acp-7-5727-2007, 2007.

Kang, E., Toohey, D. W., and Brune, W. H.: Dependence of SOA oxidation on organic aerosol mass concentration and OH exposure: experimental PAM chamber studies, Atmos. Chem. Phys., 11, 1837-1852, 10.5194/acp-11-1837-2011, 2011.

Knote, C., Hodzic, A., and Jimenez, J. L.: The effect of dry and wet deposition of condensable vapors on secondary organic aerosols concentrations over the continental US, Atmos. Chem. Phys., 15, 1-18, 10.5194/acp-15-1-2015, 2015.

Koo, B., Ansari, A. S., and Pandis, S. N.: Integrated approaches to modeling the organic and inorganic atmospheric aerosol components, Atmospheric Environment, 37, 4757-4768, http://dx.doi.org/10.1016/j.atmosenv.2003.08.016, 2003.

Kroll, J. H., Donahue, N. M., Jimenez, J. L., Kessler, S. H., Canagaratna, M. R., Wilson, K. R., Altieri, K. E., Mazzoleni, L. R., Wozniak, A. S., Bluhm, H., Mysak, E. R., Smith, J. D., Kolb, C. E., and Worsnop, D. R.: Carbon oxidation state as a metric for describing the chemistry of atmospheric organic aerosol, Nat Chem, 3, 133-139, 2011.

Kroll, J. H., Lim, C. Y., Kessler, S. H., and Wilson, K. R.: Heterogeneous Oxidation of Atmospheric Organic Aerosol: Kinetics of Changes to the Amount and Oxidation State of Particle-Phase Organic Carbon, The Journal of Physical Chemistry A, 119, 10767-10783, 10.1021/acs.jpca.5b06946, 2015.

Lambe, A. T., Ahern, A. T., Williams, L. R., Slowik, J. G., Wong, J. P. S., Abbatt, J. P. D., Brune, W. H., Ng, N. L., Wright, J. P., Croasdale, D. R., Worsnop, D. R., Davidovits, P., and Onasch, T. B.: Characterization of aerosol photooxidation flow reactors: heterogeneous oxidation, secondary organic aerosol formation and cloud condensation nuclei activity measurements, Atmos. Meas. Tech., 4, 445-461, 10.5194/amt-4-445-2011, 2011a.

Lambe, A. T., Onasch, T. B., Massoli, P., Croasdale, D. R., Wright, J. P., Ahern, A. T., Williams, L. R., Worsnop, D. R., Brune, W. H., and Davidovits, P.: Laboratory studies of the chemical composition and cloud condensation nuclei (CCN) activity of secondary organic aerosol (SOA) and oxidized primary organic aerosol (OPOA), Atmos. Chem. Phys., 11, 8913-8928, 10.5194/acp-11-8913-2011, 2011b.

Lambe, A. T., Onasch, T. B., Croasdale, D. R., Wright, J. P., Martin, A. T., Franklin, J. P., Massoli, P., Kroll, J. H., Canagaratna, M. R., Brune, W. H., Worsnop, D. R., and Davidovits, P.: Transitions from Functionalization to

Fragmentation Reactions of Laboratory Secondary Organic Aerosol (SOA) Generated from the OH Oxidation of Alkane Precursors, Environmental Science & Technology, 46, 5430–5437, 10.1021/es300274t, 2012.

Lambe, A. T., Chhabra, P. S., Onasch, T. B., Brune, W. H., Hunter, J. F., Kroll, J. H., Cummings, M. J., Brogan, J. F., Parmar, Y., Worsnop, D. R., Kolb, C. E., and Davidovits, P.: Effect of oxidant concentration, exposure time, and seed particles on secondary organic aerosol chemical composition and yield, Atmos. Chem. Phys., 15, 3063-3075, 10.5194/acp-15-3063-2015, 2015.

Li, R., Palm, B. B., Borbon, A., Graus, M., Warneke, C., Ortega, A. M., Day, D. A., Brune, W. H., Jimenez, J. L., and de Gouw, J. A.: Laboratory Studies on Secondary Organic Aerosol Formation from Crude Oil Vapors, Environmental Science & Technology, 47, 12566-12574, 10.1021/es402265y, 2013.

Li, R., Palm, B. B., Ortega, A. M., Hlywiak, J. A., Hu, W., Peng, Z., Day, D. A., Knote, C., Brune, W. H., de Gouw, J. A., and Jimenez, J. L.: Modeling the Radical Chemistry in an Oxidation Flow Reactor: Radical Formation and Recycling, Sensitivities, and OH Exposure Estimation Equation, The Journal of Physical Chemistry A, 10.1021/jp509534k, 2015.

Mao, J., Ren, X., Brune, W. H., Olson, J. R., Crawford, J. H., Fried, A., Huey, L. G., Cohen, R. C., Heikes, B., Singh, H. B., Blake, D. R., Sachse, G. W., Diskin, G. S., Hall, S. R., and Shetter, R. E.: Airborne measurement of OH reactivity during INTEX-B, Atmos. Chem. Phys., 9, 163-173, 10.5194/acp-9-163-2009, 2009.

Massoli, P., Lambe, A. T., Ahern, A. T., Williams, L. R., Ehn, M., Mikkilä, J., Canagaratna, M. R., Brune, W. H., Onasch, T. B., Jayne, J. T., Petäjä, T., Kulmala, M., Laaksonen, A., Kolb, C. E., Davidovits, P., and Worsnop, D. R.: Relationship between aerosol oxidation level and hygroscopic properties of laboratory generated secondary organic aerosol (SOA) particles, Geophys. Res. Lett., 37, L24801, 10.1029/2010gl045258, 2010.

McMurry, P. H., and Grosjean, D.: Gas and aerosol wall losses in Teflon film smog chambers, Environmental Science & Technology, 19, 1176-1182, 10.1021/es00142a006, 1985.

Morino, Y., Tanabe, K., Sato, K., and Ohara, T.: Secondary organic aerosol model intercomparison based on secondary organic aerosol to odd oxygen ratio in Tokyo, Journal of Geophysical Research: Atmospheres, 119, 2014JD021937, 10.1002/2014jd021937, 2014.

Murphy, D. M., Cziczo, D. J., Froyd, K. D., Hudson, P. K., Matthew, B. M., Middlebrook, A. M., Peltier, R. E., Sullivan, A., Thomson, D. S., and Weber, R. J.: Single-particle mass spectrometry of tropospheric aerosol particles, Journal of Geophysical Research: Atmospheres, 111, D23S32, 10.1029/2006jd007340, 2006.

Myhre, G., Shindell, D., Bréon, F.-M., Collins, W., Fuglestvedt, J., Huang, J., Koch, D., Lamarque, J.-F., Lee, D., Mendoza, B., Nakajima, T., Robock, A., Stephens, G., Takemura, T., and Zhang, H.: Anthropogenic and Natural Radiative Forcing, in Climate Change 2013: The Physical Science Basis. Contribution of Working Group I to the Fifth Assessment Report of the Intergovernmental Panel on Climate Change, edited by V. B. and P. M. M. Stocker, T.F., D. Qin, G.-K. Plattner, M. Tignor, S.K. Allen, J. Boschung, A. Nauels, Y. Xia, Cambridge University Press, Cambridge, United Kingdom and New York, NY, USA., 2013.

Ng, N. L., Canagaratna, M. R., Zhang, Q., Jimenez, J. L., Tian, J., Ulbrich, I. M., Kroll, J. H., Docherty, K. S., Chhabra, P. S., Bahreini, R., Murphy, S. M., Seinfeld, J. H., Hildebrandt, L., Donahue, N. M., DeCarlo, P. F., Lanz, V. A., Prévôt, A. S. H., Dinar, E., Rudich, Y., and Worsnop, D. R.: Organic aerosol components observed in Northern Hemispheric datasets from Aerosol Mass Spectrometry, Atmos. Chem. Phys., 10, 4625-4641, 10.5194/acp-10-4625-2010, 2010.

Ng, N. L., Canagaratna, M. R., Jimenez, J. L., Chhabra, P. S., Seinfeld, J. H., and Worsnop, D. R.: Changes in organic aerosol composition with aging inferred from aerosol mass spectra, Atmos Chem Phys, 11, 6465-6474, 2011a.

Ng, N. L., Canagaratna, M. R., Jimenez, J. L., Zhang, Q., Ulbrich, I. M., and Worsnop, D. R.: Real-Time Methods for Estimating Organic Component Mass Concentrations from Aerosol Mass Spectrometer Data, Environ Sci Technol, 45, 910-916, 2011b.

Ortega, A. M., Day, D. A., Cubison, M. J., Brune, W. H., Bon, D., de Gouw, J. A., and Jimenez, J. L.: Secondary organic aerosol formation and primary organic aerosol oxidation from biomass-burning smoke in a flow reactor during FLAME-3, Atmos. Chem. Phys., 13, 11551-11571, 10.5194/acp-13-11551-2013, 2013.

Palm, B. B., Campuzano-Jost, P., Ortega, A. M., Day, D. A., Kaser, L., Jud, W., Karl, T., Hansel, A., Hunter, J. F., Cross, E. S., Kroll, J. H., Peng, Z., Brune, W. H., and Jimenez, J. L.: In situ secondary organic aerosol formation from ambient pine forest air using an oxidation flow reactor, Atmos. Chem. Phys., 16, 2943-2970, 10.5194/acp-16-2943-2016, 2016.

Pankow, J. F.: An absorption model of gas/particle partitioning of organic compounds in the atmosphere, Atmospheric Environment, 28, 185-188, http://dx.doi.org/10.1016/1352-2310(94)90093-0, 1994.

Peng, Z., Day, D. A., Stark, H., Li, R., Lee-Taylor, J., Palm, B. B., Brune, W. H., and Jimenez, J. L.: HOx radical chemistry in oxidation flow reactors with low-pressure mercury lamps systematically examined by modeling, Atmos. Meas. Tech., 8, 4863-4890, 10.5194/amt-8-4863-2015, 2015.

Peng, Z., Day, D. A., Ortega, A. M., Palm, B. B., Hu, W. W., Stark, H., Li, R., Tsigaridis, K., Brune, W. H., and Jimenez, J. L.: Non-OH chemistry in oxidation flow reactors for the study of atmospheric chemistry systematically examined by modeling, Atmos. Chem. Phys., 2016, 4283-4305, 10.5194/acp-16-4283-2016, 2016.

Phousongphouang, P. T., and Arey, J.: Rate Constants for the Gas-Phase Reactions of a Series of Alkylnaphthalenes with the OH Radical, Environ Sci Technol, 36, 1947-1952, 10.1021/es011434c, 2002.

Pirjola, L., Kulmala, M., Wilck, M., Bischoff, A., Stratmann, F., and Otto, E.: Formation of Sulphuric Acid Aerosols and Cloud COndensation Nuclei: An Expresion for Significant Nucleation and Model Comprarison, Journal of Aerosol Science, 30, 1079-1094, http://dx.doi.org/10.1016/S0021-8502(98)00776-9, 1999.

Pope, C. A., Burnett, R. T., Thun, M. J., Calle, E. E., Krewski, D., Ito, K., and Thurston, G. D.: Lung cancer, cardiopulmonary mortality, and long-term exposure to fine particulate air pollution, Jama-Journal of the American Medical Association, 287, 1132-1141, 10.1001/jama.287.9.1132, 2002.

Reutter, P., Su, H., Trentmann, J., Simmel, M., Rose, D., Gunthe, S. S., Wernli, H., Andreae, M. O., and Pöschl, U.: Aerosol- and updraft-limited regimes of cloud droplet formation: influence of particle number, size and hygroscopicity on the activation of cloud condensation nuclei (CCN), Atmos. Chem. Phys., 9, 7067-7080, 10.5194/acp-9-7067-2009, 2009.

Robinson, A. L., Donahue, N. M., Shrivastava, M. K., Weitkamp, E. A., Sage, A. M., Grieshop, A. P., Lane, T. E., Pierce, J. R., and Pandis, S. N.: Rethinking Organic Aerosols: Semivolatile Emissions and Photochemical Aging, Science, 315, 1259-1262, 10.1126/science.1133061, 2007.

Ryerson, T. B., Andrews, A. E., Angevine, W. M., Bates, T. S., Brock, C. A., Cairns, B., Cohen, R. C., Cooper, O. R., de Gouw, J. A., Fehsenfeld, F. C., Ferrare, R. A., Fischer, M. L., Flagan, R. C., Goldstein, A. H., Hair, J. W., Hardesty, R. M., Hostetler, C. A., Jimenez, J. L., Langford, A. O., McCauley, E., McKeen, S. A., Molina, L. T., Nenes, A., Oltmans, S. J., Parrish, D. D., Pederson, J. R., Pierce, R. B., Prather, K., Quinn, P. K., Seinfeld, J. H., Senff, C. J., Sorooshian, A., Stutz, J., Surratt, J. D., Trainer, M., Volkamer, R., Williams, E. J., and Wofsy, S. C.: The 2010 California Research at the Nexus of Air Quality and Climate Change (CalNex) field study, Journal of Geophysical Research: Atmospheres, 118, 5830-5866, 10.1002/jgrd.50331, 2013.

Tkacik, D. S., Lambe, A. T., Jathar, S., Li, X., Presto, A. A., Zhao, Y., Blake, D., Meinardi, S., Jayne, J. T., Croteau, P. L., and Robinson, A. L.: Secondary Organic Aerosol Formation from in-Use Motor Vehicle Emissions Using a Potential Aerosol Mass Reactor, Environmental Science & Technology, 48, 11235-11242, 10.1021/es502239v, 2014.

Tsimpidi, A. P., Karydis, V. A., Zavala, M., Lei, W., Molina, L., Ulbrich, I. M., Jimenez, J. L., and Pandis, S. N.: Evaluation of the volatility basis-set approach for the simulation of organic aerosol formation in the Mexico City metropolitan area, Atmos. Chem. Phys., 10, 525-546, 10.5194/acp-10-525-2010, 2010.

Vaden, T. D., Imre, D., Beránek, J., Shrivastava, M., and Zelenyuk, A.: Evaporation kinetics and phase of laboratory and ambient secondary organic aerosol, Proceedings of the National Academy of Sciences, 108, 2190-2195, 10.1073/pnas.1013391108, 2011.

Volkamer, R., Jimenez, J. L., San Martini, F., Dzepina, K., Zhang, Q., Salcedo, D., Molina, L. T., Worsnop, D. R., and Molina, M. J.: Secondary organic aerosol formation from anthropogenic air pollution: Rapid and higher than expected, Geophys. Res. Lett., 33, L17811, 10.1029/2006gl026899, 2006.

Warneke, C., de Gouw, J. A., Edwards, P. M., Holloway, J. S., Gilman, J. B., Kuster, W. C., Graus, M., Atlas, E., Blake, D., Gentner, D. R., Goldstein, A. H., Harley, R. A., Alvarez, S., Rappenglueck, B., Trainer, M., and Parrish, D. D.: Photochemical aging of volatile organic compounds in the Los Angeles basin: Weekday-weekend effect, Journal of Geophysical Research: Atmospheres, 118, 5018-5028, 10.1002/jgrd.50423, 2013.

Washenfelder, R. A., Young, C. J., Brown, S. S., Angevine, W. M., Atlas, E. L., Blake, D. R., Bon, D. M., Cubison, M. J., de Gouw, J. A., Dusanter, S., Flynn, J., Gilman, J. B., Graus, M., Griffith, S., Grossberg, N., Hayes, P. L., Jimenez, J. L., Kuster, W. C., Lefer, B. L., Pollack, I. B., Ryerson, T. B., Stark, H., Stevens, P. S., and Trainer, M. K.: The glyoxal budget and its contribution to organic aerosol for Los Angeles, California, during CalNex 2010, Journal of Geophysical Research: Atmospheres, 116, D00V02, 10.1029/2011jd016314, 2011.

Watson, J. G.: Visibility: Science and regulation, Journal of the Air & Waste Management Association, 52, 628-713, 2002.

Wood, E. C., Canagaratna, M. R., Herndon, S. C., Onasch, T. B., Kolb, C. E., Worsnop, D. R., Kroll, J. H., Knighton, W. B., Seila, R., Zavala, M., Molina, L. T., DeCarlo, P. F., Jimenez, J. L., Weinheimer, A. J., Knapp, D. J., Jobson, B. T., Stutz, J., Kuster, W. C., and Williams, E. J.: Investigation of the correlation between odd oxygen and secondary organic aerosol in Mexico City and Houston, Atmos. Chem. Phys., 10, 8947-8968, 10.5194/acp-10-8947-2010, 2010.

Zhang, Q., Jimenez, J. L., Canagaratna, M. R., Allan, J. D., Coe, H., Ulbrich, I., Alfarra, M. R., Takami, A., Middlebrook, A. M., Sun, Y. L., Dzepina, K., Dunlea, E., Docherty, K., DeCarlo, P. F., Salcedo, D., Onasch, T., Jayne, J. T., Miyoshi, T., Shimono, A., Hatakeyama, S., Takegawa, N., Kondo, Y., Schneider, J., Drewnick, F., Borrmann, S., Weimer, S., Demerjian, K., Williams, P., Bower, K., Bahreini, R., Cottrell, L., Griffin, R. J., Rautiainen, J., Sun, J. Y., Zhang, Y. M., and Worsnop, D. R.: Ubiquity and dominance of oxygenated species in organic aerosols in anthropogenically-influenced Northern Hemisphere midlatitudes, Geophys. Res. Lett., 34, L13801, 10.1029/2007gl029979, 2007.

Zhang, Q. J., Beekmann, M., Freney, E., Sellegri, K., Pichon, J. M., Schwarzenboeck, A., Colomb, A., Bourrianne, T., Michoud, V., and Borbon, A.: Formation of secondary organic aerosol in the Paris pollution plume and its impact on surrounding regions, Atmos. Chem. Phys. Discuss., 15, 8073-8111, 10.5194/acpd-15-8073-2015, 2015.

Zhang, X., Cappa, C. D., Jathar, S. H., McVay, R. C., Ensberg, J. J., Kleeman, M. J., and Seinfeld, J. H.: Influence of vapor wall loss in laboratory chambers on yields of secondary organic aerosol, Proceedings of the National Academy of Sciences, 111, 5802-5807, 10.1073/pnas.1404727111, 2014.

Zhao, Y., Hennigan, C. J., May, A. A., Tkacik, D. S., de Gouw, J. A., Gilman, J. B., Kuster, W. C., Borbon, A., and Robinson, A. L.: Intermediate-Volatility Organic Compounds: A Large Source of Secondary Organic Aerosol, Environmental Science & Technology, 48, 13743-13750, 10.1021/es5035188, 2014.

Ziemann, P. J., and Atkinson, R.: Kinetics, products, and mechanisms of secondary organic aerosol formation, Chemical Society Reviews, 41, 6582-6605, 10.1039/c2cs35122f, 2012.

Figure Captions

Figure 1: (a) Schematic of the oxidation flow reactor (OFR) coupled to an Aerodyne high-resolution time-of-flight aerosol mass spectrometer (AMS), scanning-mobility particle sizer (SMPS), and ozone (O_3) monitor. An ambient sampling line allowed for direct sampling of ambient air. Computer-controlled switching valves allowed for sampling in alternation from the reactor and ambient lines. Voltage supplied to UV lamps were varied via programmable computer control to step through oxidant concentrations in the reactor. Ring flow was via a PTFE Teflon line and was used for gas-phase measurements. Center flow was a copper line that continuously pulled the sample for aerosol analysis. **(b)** Photograph of the reactor with a sun / rain cover and of the ambient aerosol inlet (right, covered by foil insulation) on the trailer roof during CalNex. **(c)** Photograph of the sampling site showing the different trailers and inlets. The OFR can be seen on top of the leftmost trailer, next to the AMS and SMPS ambient inlets.

Figure 2: A typical OFR sampling cycle, including four steps in lamp intensity in the reactor. Top: reactor oxidant concentrations. Bottom: OA concentration for ambient and reactor output sampling. The UV light intensity color scale corresponds to the sum of the AC voltages applied to the two lamps in the reactor. Only at the highest lamp setting are both lamps on, while at lower settings only one of the lamps is used.

Figure 3: (a) Time series of reactor and ambient species mass concentrations during the sampling period. **(b)** Zoom on the time series of the species mass concentrations for one representative day. Daytime and nighttime are marked. **(c)** Average fraction contribution from organic, nitrate, sulfate, ammonium, and chloride to total AMS aerosol measurements for ambient and reactor (excluding dark reactor, “lights off” periods, i.e. periods are included only if OH_{exp} > ambient). The pie chart areas are proportional to the total mass concentrations.

Figure 4: (a) Relative OA enhancement (ER_{OA} = reactor OA / ambient OA) vs.estimated reactor photochemical age for the sampling period. **(b)** Absolute OA mass concentration enhancement (ΔOA Mass = reactor OA - ambient OA) versus photochemical age. The data has been averaged into 6% quantiles for day and night measurements, with vertical error bars indicating standard errors.

Figure 5: Reactor OA mass enhancement vs. ambient O_x, (odd oxygen; O_3+NO_2) for all data in ~3.7 and ~23.5 day reactor age ranges during the sample period, colored by nighttime and daytime. Average for 10% quantiles are shown for ~3.7 days and ~23.5 days of photochemical age, with error bars indicating standard errors. Note that ambient O_x is not itself playing a role in reactor aging, but rather is a proxy for ambient photochemistry.

Figure 6: Times series of benzene, 1,3,5-trimethylbenzene, ambient total oxygenated organic aerosol (OOA), reactor organic mass enhancement, and maximum reactor organic mass enhancement. Inset is a scatter plot of maximum reactor OA mass enhancement (for each OH_{exp} cycle) vs. ambient 1,3,5-trimethylbenzene, with a linear ODR regression fit.

Figure 7: (a) Fractional contribution of *m/z* 44 (f_{44}) vs. *m/z* 43 (f_{43}) to OA for the ambient and reactor data in this work. The region of ambient observations from Ng et al. (2011b), and for reactor laboratory observations and oxalic acid from Lambe et al. (2011a) are shown. **(b)** Van Krevelen diagram for ambient and reactor measurements for the sampling period. Functionalization slopes from Heald et al. (2010), and oxidation state from Kroll et al. (2011) are shown for reference. Elemental analysis has been calculated with the Improved-Ambient method from Canagaratna et al. (2015). Reactor measurements are colored by total photochemical age in days (at OH = 1.5×10^6 molec. cm^{-3}) and ambient PMF-derived HOA, SV- and LV-OOA factors are shown from Hayes et al. (2013).

Figure 8: (a) Oxygen-to-carbon (O:C) and **(b)** hydrogen-to-carbon (H:C) elemental ratios for OA mass measured from the reactor vs. total photochemical age in days (at OH = 1.5×10^6 molec. cm^{-3}). Results using similar reactors for alkane oxidation from Lambe et al. (2012), and for aging of biomass burning smoke (Ortega et al., 2013) are also shown. **(c)** Average oxidation state (OS_C= 2O:C – H:C) vs. OH_{exp}. Data are colored by the relative organic enhancement (ER_{OA} = reactor OA / ambient OA).

Figure 9: Ratio of OA to excess carbon monoxide (above background levels) vs. total photochemical age in days (at OH = 1.5×10^6 molec. cm^{-3}) for ambient and reactor data, with vertical error bars indicating standard errors. Also shown in the value for LA Basin outflow from aircraft measurements from the NOAA WP-3D during CalNex (Bahreini et al., 2012b). See Hayes et al. (2013) for a discussion of the determination of CO background levels. Averages for quantiles of ambient (7%), reactor (7%), reactor dark (25%, internal OH_{exp}= 0) and reactor vapor loss-corrected (12%) data are shown. A fit to reactor data is also shown, including background (BG) SOA, and primary organic aerosol (POA;see text for details). Results from field studies in

the northeastern US and Mexico City are shown in the background (DeCarlo et al., 2010). Note that the LVOC loss correction can only be applied when reactor output OA is larger than ambient OA, which reduces the number of datapoints.

Figure 10: R^2 between the concentrations of different VOCs and the maximum amount of SOA formation in the OFR, plotted vs. the reaction rate constant of each VOC with OH (k_{OH}).

Figure 11: Comparison of reactor data with model results for evolution of OA/ΔCO vs. total photochemical age in days (at OH = 1.5×10^6 molec. cm^{-3}) with **(a)** traditional SOA formation model, high NO_x Robinson + Tsimpidi model from Hayes et al. (2015). Also shown is the summary of urban aged ratios from de Gouw and Jimenez (2009). **(b)** High NO_x Robinson + Tsimpidi model from Hayes et al. (2015) run with one-half IVOCs per the results of Zhao et al. (2014). (POA+BGSOA)/ΔCO is 21 μg m^{-3} ppm^{-1}, which somewhat is higher than the value of 16 μg m^{-3} ppm^{-1} previously reported by Hayes et al. (2013).

Figure 12: **(a)** Relative organic aerosol enhancement (ER_{OA}) from all reactor data in this study (including 6% quantiles), with vertical error bars indicating standard errors, and from a heterogeneous oxidation study (George and Abbatt, 2010) plotted vs. total photochemical age in days (at OH = 1.5×10^6 molec. cm^{-3}). **(b)** SOA/ΔCO vs. photochemical age for our study and for aging of vehicle exhaust with a similar reactor at a tunnel near Pittsburgh, PA (Tkacik et al., 2014). Results from field studies in the northeastern US and Mexico City are shown in the background (DeCarlo et al., 2010).

Figure 1.

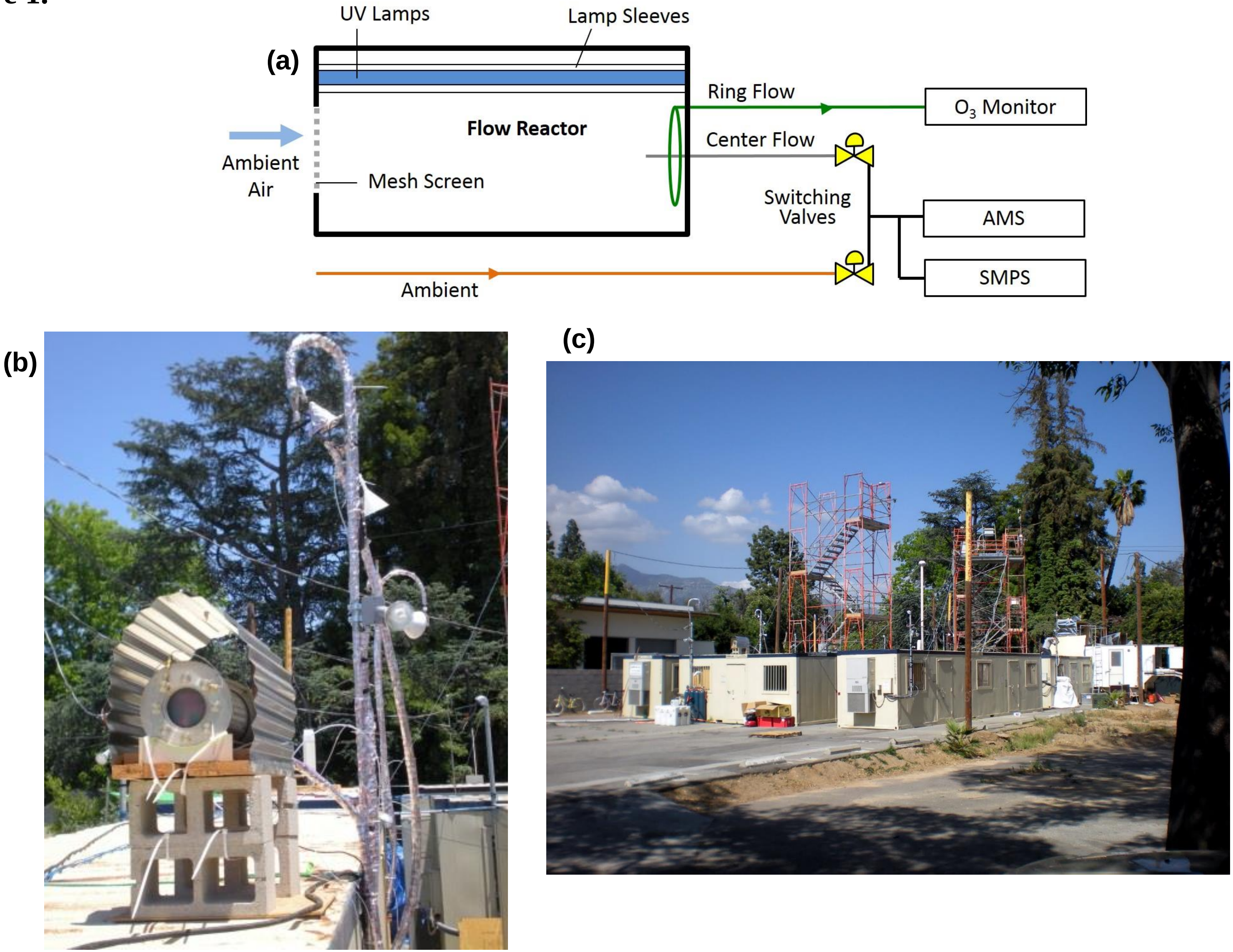
(a)
UV Lamps
Lamp Sleeves
Ring Flow
O_3 Monitor
Flow Reactor
Center Flow
Ambient
Air
Mesh Screen
Switching
Valves
AMS
SMPS
Ambient
(b)
(c)

Figure 2.

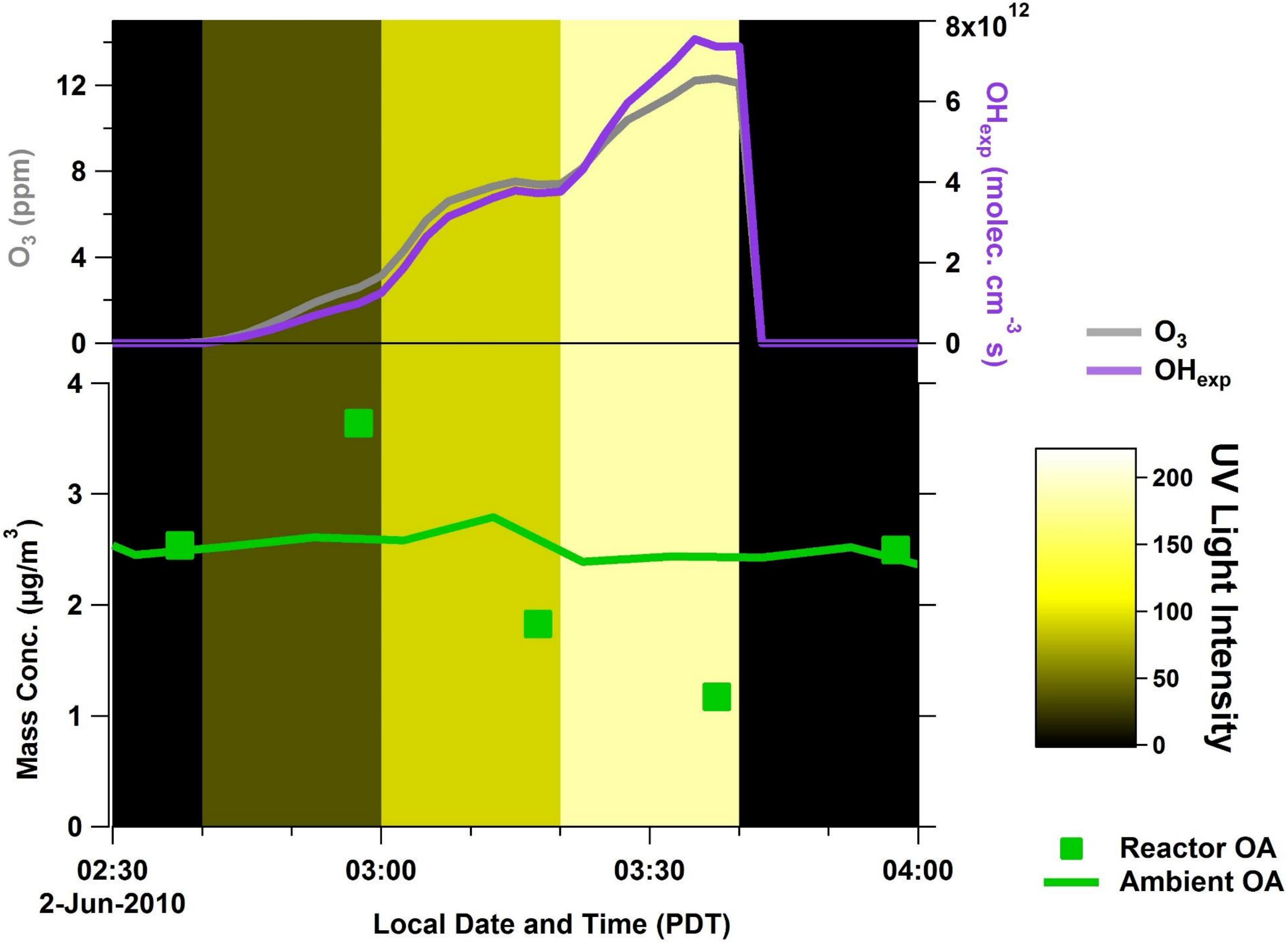

O$_3$ (ppm)
12
8
4
0
8x10^{12}
6
4
2
0
OH$_{exp}$ (molec. cm^{-3} s)
O$_3$
OH$_{exp}$
Mass Conc. (µg/m^3)
4
3
2
1
0
UV Light Intensity
200
150
100
50
0
02:30
2-Jun-2010
03:00
03:30
04:00
Local Date and Time (PDT)
Reactor OA
Ambient OA

Figure 3.

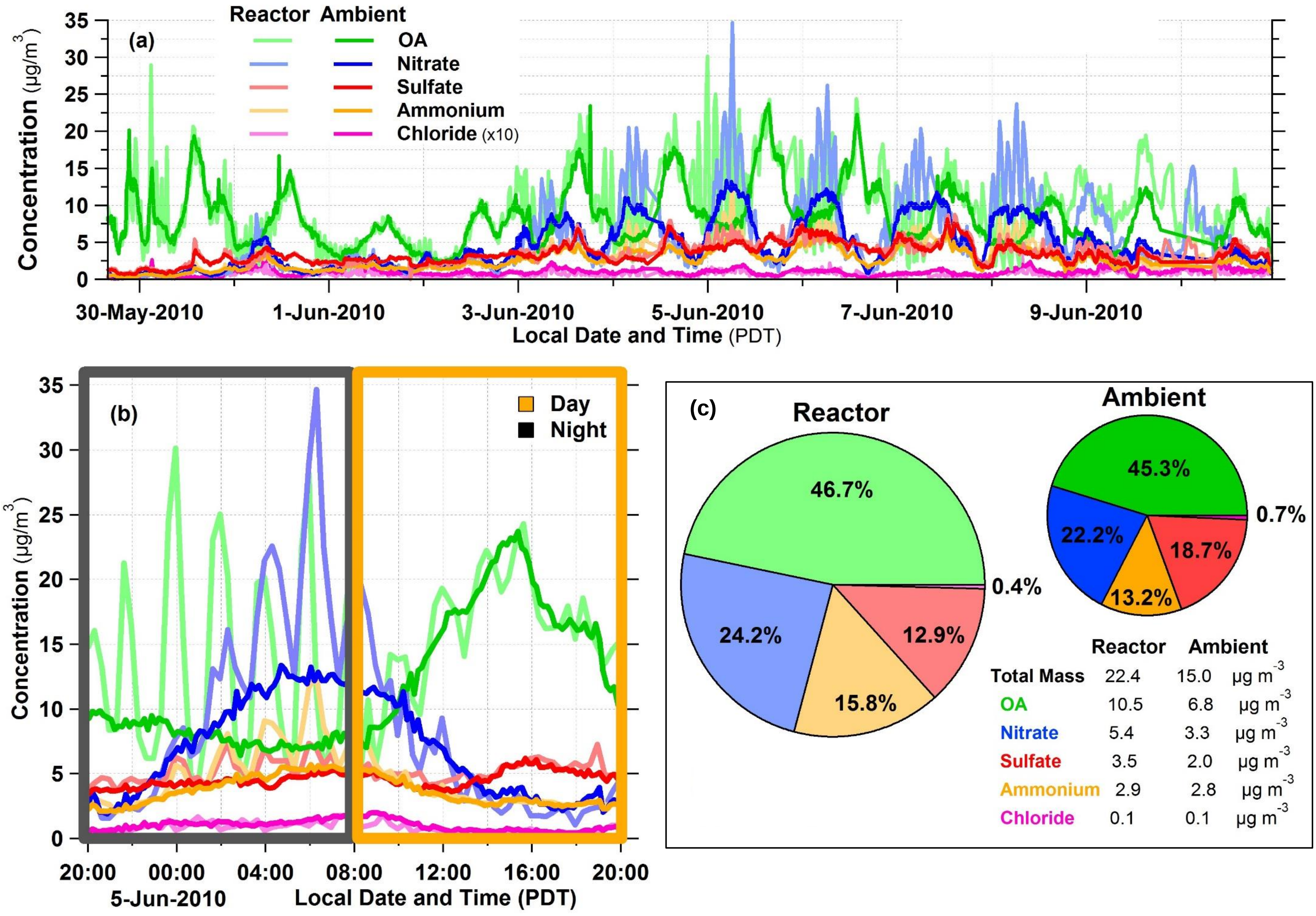

	Reactor	Ambient	
Total Mass	22.4	15.0	μg m^{-3}
OA	10.5	6.8	μg m^{-3}
Nitrate	5.4	3.3	μg m^{-3}
Sulfate	3.5	2.0	μg m^{-3}
Ammonium	2.9	2.8	μg m^{-3}
Chloride	0.1	0.1	μg m^{-3}

Figure 4.

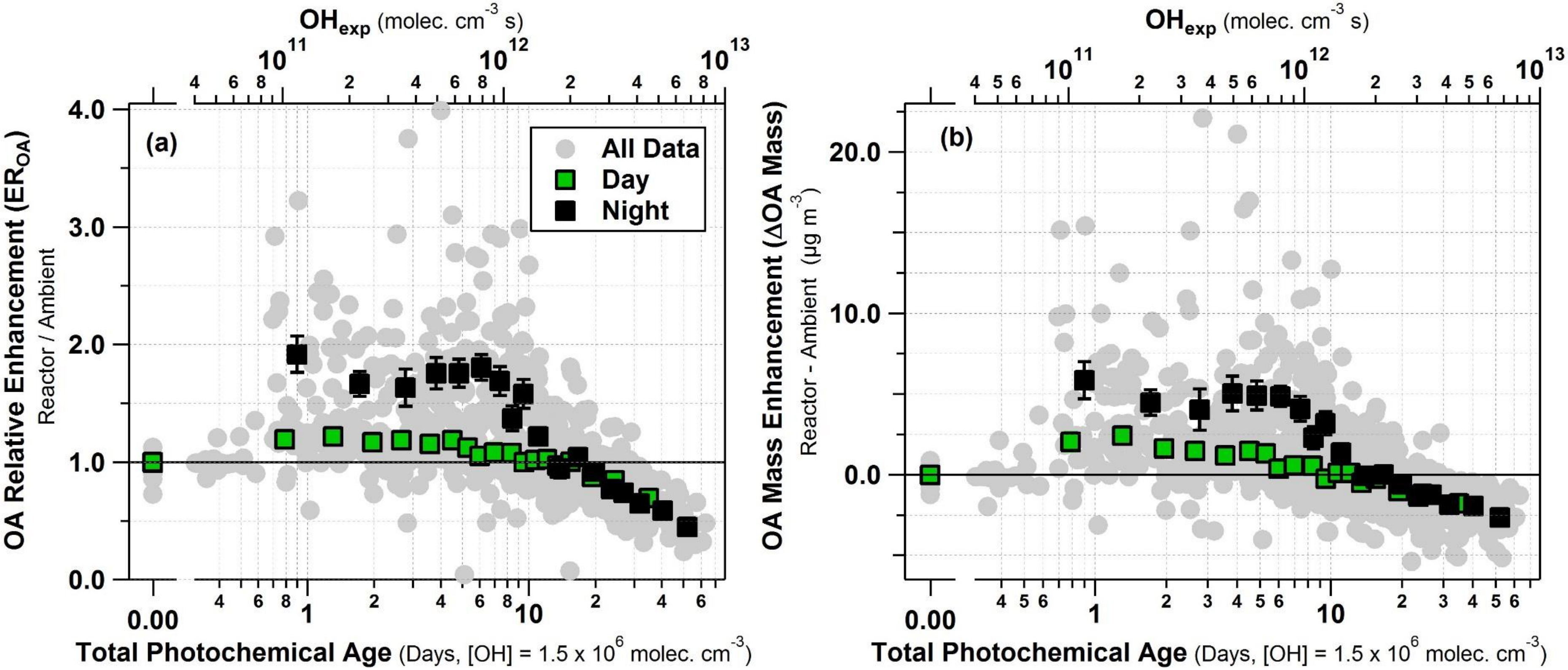
OH$_{exp}$ (molec. cm^{-3} s)
(a)
(b)
All Data
Day
Night
OA Relative Enhancement (ER$_{OA}$)
Reactor / Ambient
OA Mass Enhancement (ΔOA Mass)
Reactor - Ambient (μg m^{-3})
Total Photochemical Age (Days, [OH] = 1.5 x 10^6 molec. cm^{-3})
0.00
4.0
3.0
2.0
1.0
0.0
20.0
10.0
0.0
10^{11}
10^{12}
10^{13}
1
10

Figure 5.

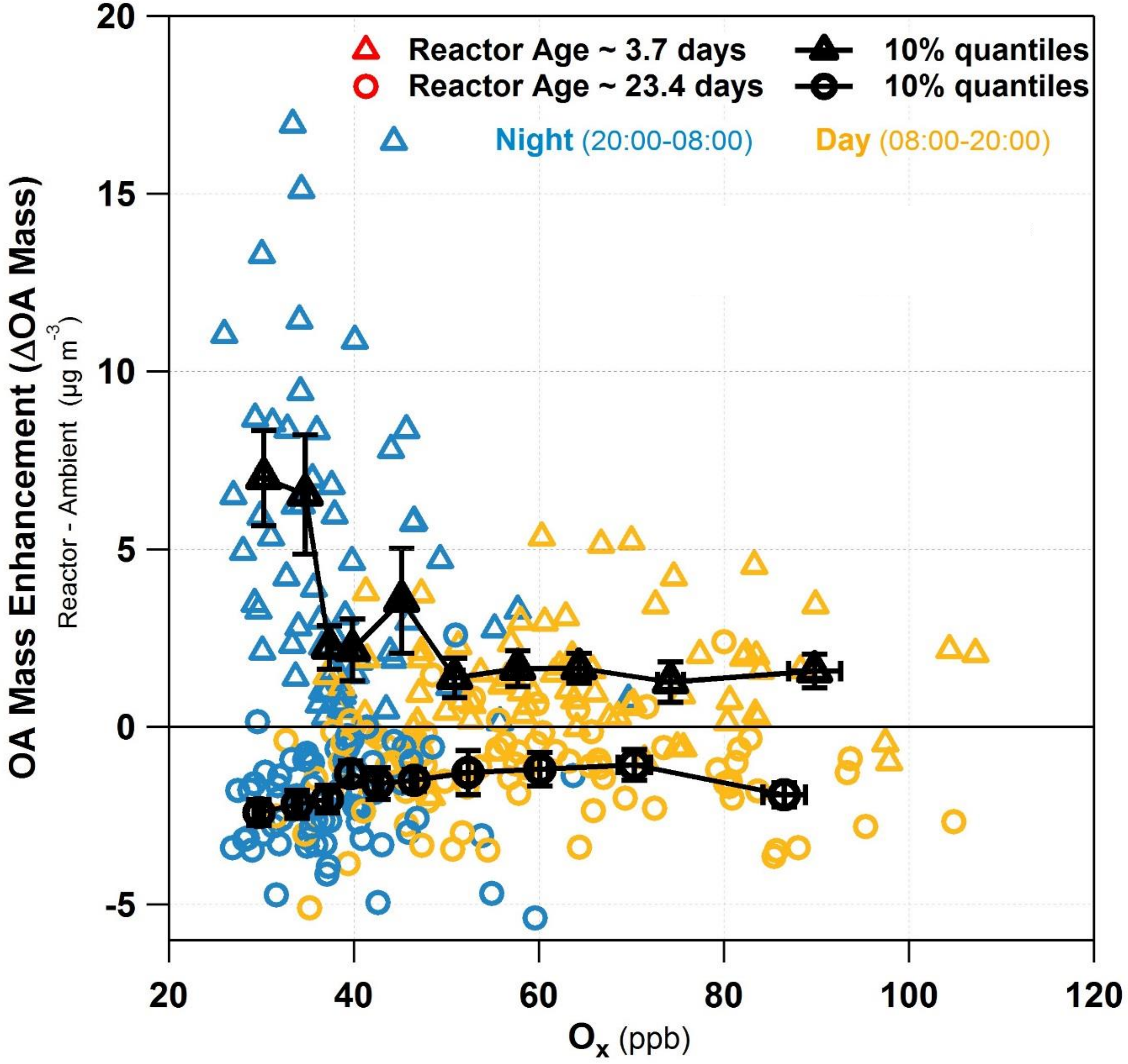
Reactor Age ~ 3.7 days
Reactor Age ~ 23.4 days
10% quantiles
10% quantiles
Night (20:00-08:00)
Day (08:00-20:00)
OA Mass Enhancement (ΔOA Mass)
Reactor - Ambient (μg m^{-3})
20
15
10
5
0
-5
20
40
60
80
100
120
O$_x$ (ppb)

Figure 6.

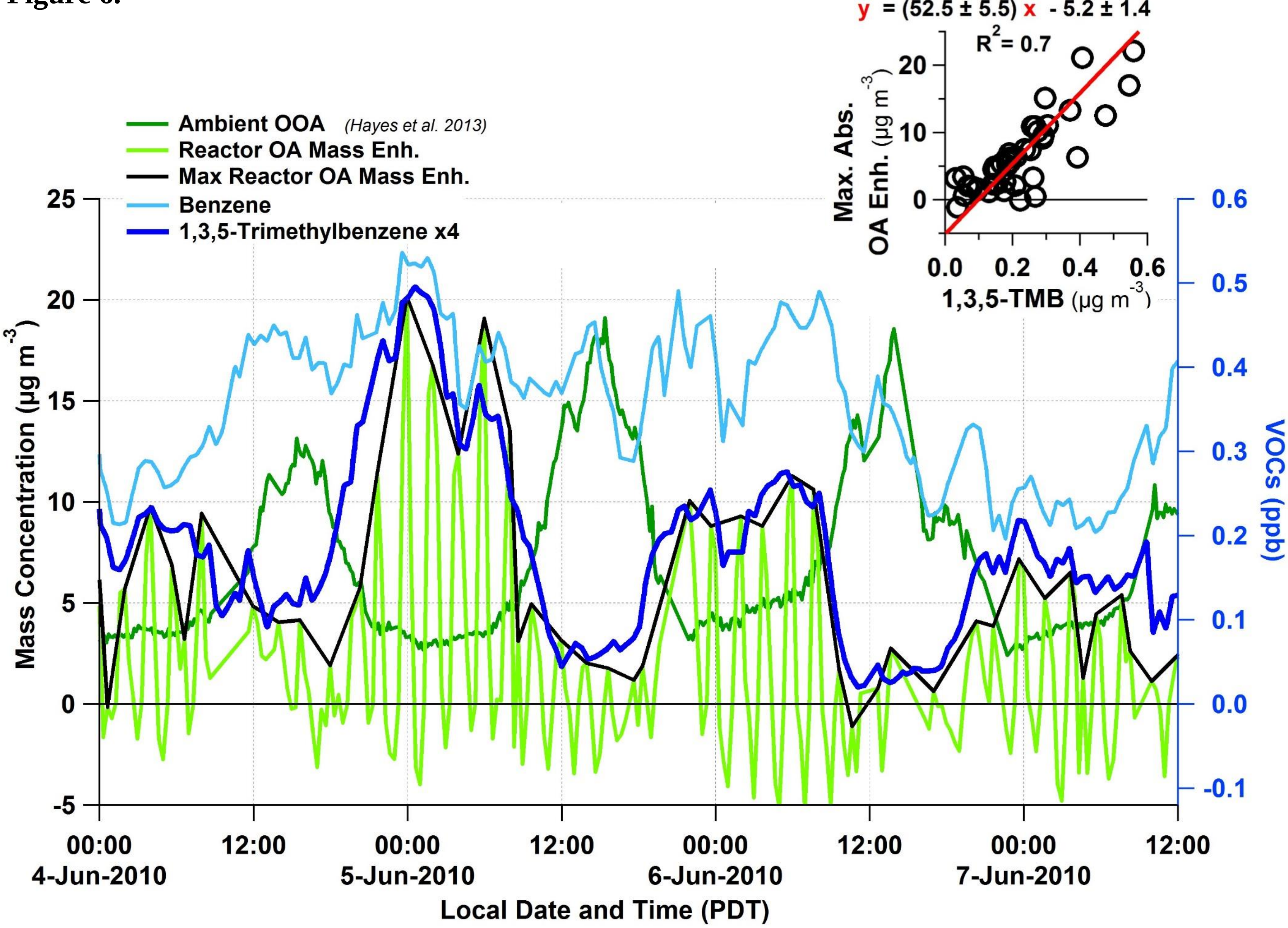

y = (52.5 ± 5.5) x - 5.2 ± 1.4
R^2= 0.7
Max. Abs. OA Enh. (µg m^{-3})
1,3,5-TMB (µg m^{-3})
0.0
0.2
0.4
0.6
20
10
0
Ambient OOA (Hayes et al. 2013)
Reactor OA Mass Enh.
Max Reactor OA Mass Enh.
Benzene
1,3,5-Trimethylbenzene x4
Mass Concentration (µg m^{-3})
25
20
15
10
5
0
-5
VOCs (ppb)
0.6
0.5
0.4
0.3
0.2
0.1
0.0
-0.1
00:00 4-Jun-2010
12:00
00:00 5-Jun-2010
12:00
00:00 6-Jun-2010
12:00
00:00 7-Jun-2010
12:00
Local Date and Time (PDT)

Figure 7.

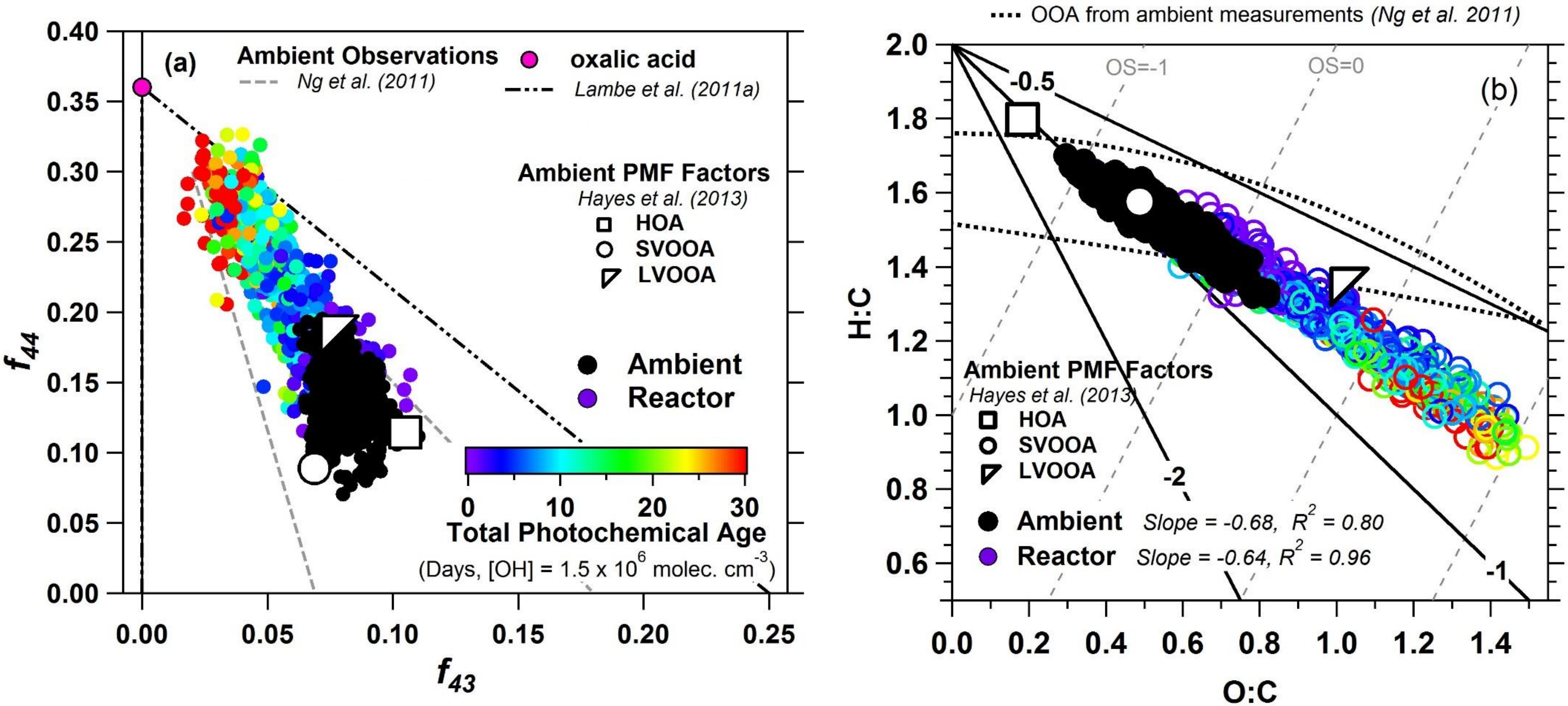

(a)
Ambient Observations
Ng et al. (2011)
oxalic acid
Lambe et al. (2011a)
Ambient PMF Factors
Hayes et al. (2013)
HOA
SVOOA
LVOOA
Ambient
Reactor
0
10
20
30
Total Photochemical Age
(Days, [OH] = 1.5 x 10^{6} molec. cm^{-3})
0.40
0.35
0.30
0.25
0.20
0.15
0.10
0.05
0.00
f_{44}
0.00
0.05
0.10
0.15
0.20
0.25
f_{43}
OOA from ambient measurements (Ng et al. 2011)
(b)
OS=-1
OS=0
-0.5
-2
-1
Ambient PMF Factors
Hayes et al. (2013)
HOA
SVOOA
LVOOA
Ambient Slope = -0.68, R^2 = 0.80
Reactor Slope = -0.64, R^2 = 0.96
2.0
1.8
1.6
1.4
1.2
1.0
0.8
0.6
H:C
0.0
0.2
0.4
0.6
0.8
1.0
1.2
1.4
O:C

Figure 8.

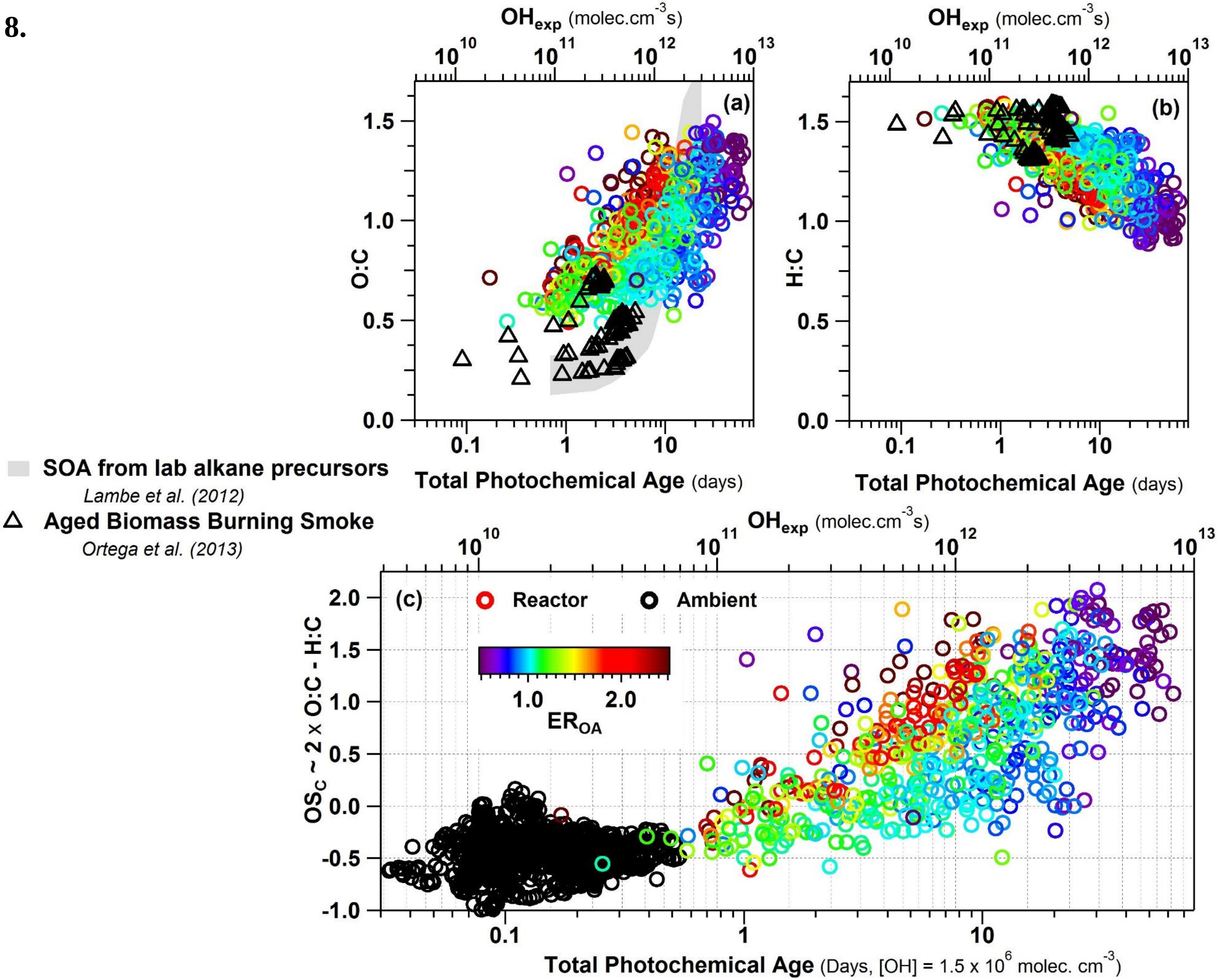
SOA from lab alkane precursors
Lambe et al. (2012)
Aged Biomass Burning Smoke
Ortega et al. (2013)
(a)
O:C
OH$_{exp}$ (molec.cm^{-3}s)
10^{10}
10^{11}
10^{12}
10^{13}
1.5
1.0
0.5
0.0
0.1
1
10
Total Photochemical Age (days)
(b)
H:C
OH$_{exp}$ (molec.cm^{-3}s)
Total Photochemical Age (days)
(c)
Reactor
Ambient
1.0
2.0
ER$_{OA}$
OS$_C$ ~ 2 x O:C - H:C
2.0
1.5
1.0
0.5
0.0
-0.5
-1.0
OH$_{exp}$ (molec.cm^{-3}s)
Total Photochemical Age (Days, [OH] = 1.5 x 10^6 molec. cm^{-3})

Figure 9.

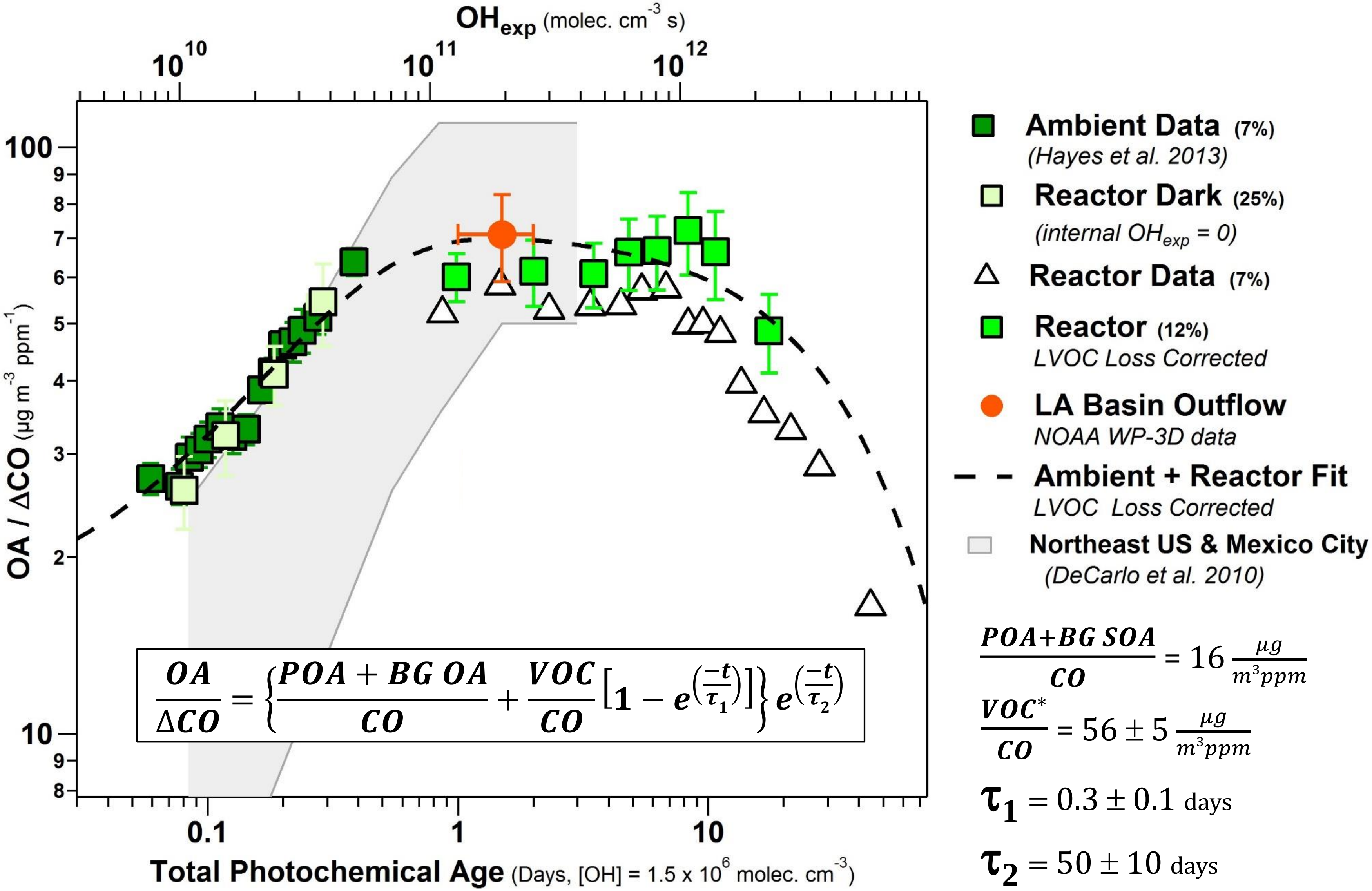

$$\frac{OA}{\Delta CO} = \left\{\frac{POA + BG\ OA}{CO} + \frac{VOC}{CO}\left[1 - e^{\left(\frac{-t}{\tau_1}\right)}\right]\right\} e^{\left(\frac{-t}{\tau_2}\right)}$$

$$\frac{POA+BG\ SOA}{CO} = 16\ \frac{\mu g}{m^3 ppm}$$

$$\frac{VOC^*}{CO} = 56 \pm 5\ \frac{\mu g}{m^3 ppm}$$

$$\tau_1 = 0.3 \pm 0.1 \text{ days}$$

$$\tau_2 = 50 \pm 10 \text{ days}$$

Figure 10.

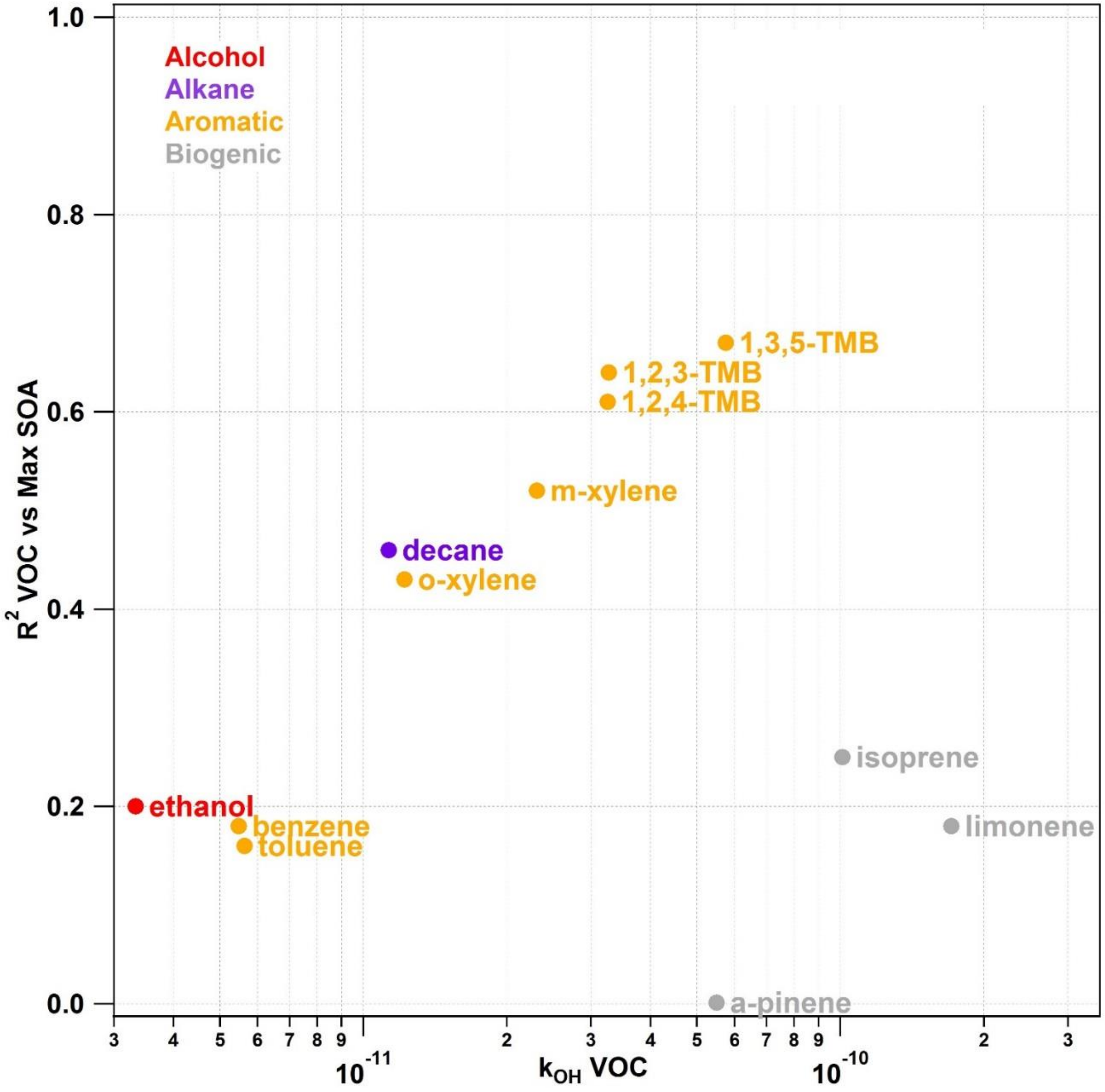

Alcohol
Alkane
Aromatic
Biogenic
1,3,5-TMB
1,2,3-TMB
1,2,4-TMB
m-xylene
decane
o-xylene
isoprene
ethanol
benzene
toluene
limonene
a-pinene
1.0
0.8
0.6
0.4
0.2
0.0
R^2 VOC vs Max SOA
3
4
5
6
7
8
9
10^{-11}
2
3
4
5
6
7
8
9
10^{-10}
2
3
k_{OH} VOC

Figure 11.

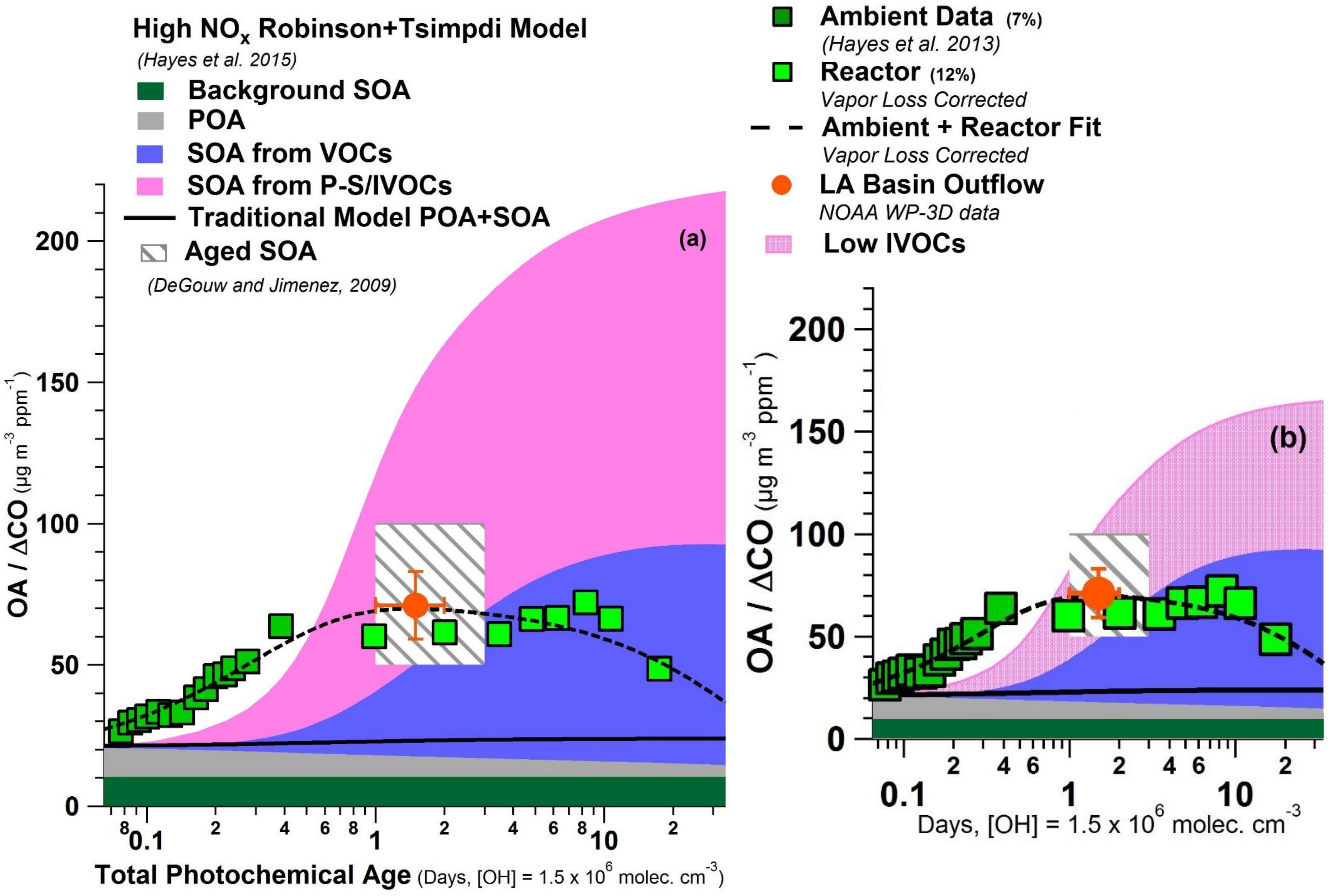
High NOx Robinson+Tsimpdi Model
(Hayes et al. 2015)
Background SOA
POA
SOA from VOCs
SOA from P-S/IVOCs
Traditional Model POA+SOA
Aged SOA
(DeGouw and Jimenez, 2009)
Ambient Data (7%)
(Hayes et al. 2013)
Reactor (12%)
Vapor Loss Corrected
Ambient + Reactor Fit
Vapor Loss Corrected
LA Basin Outflow
NOAA WP-3D data
Low IVOCs
(a)
(b)
OA / ΔCO (µg m-3 ppm-1)
0
50
100
150
200
8
0.1
2
4
6
8
1
2
4
6
8
10
2
Total Photochemical Age (Days, [OH] = 1.5 x 10^6 molec. cm-3)
Days, [OH] = 1.5 x 10^6 molec. cm-3

Figure 12.

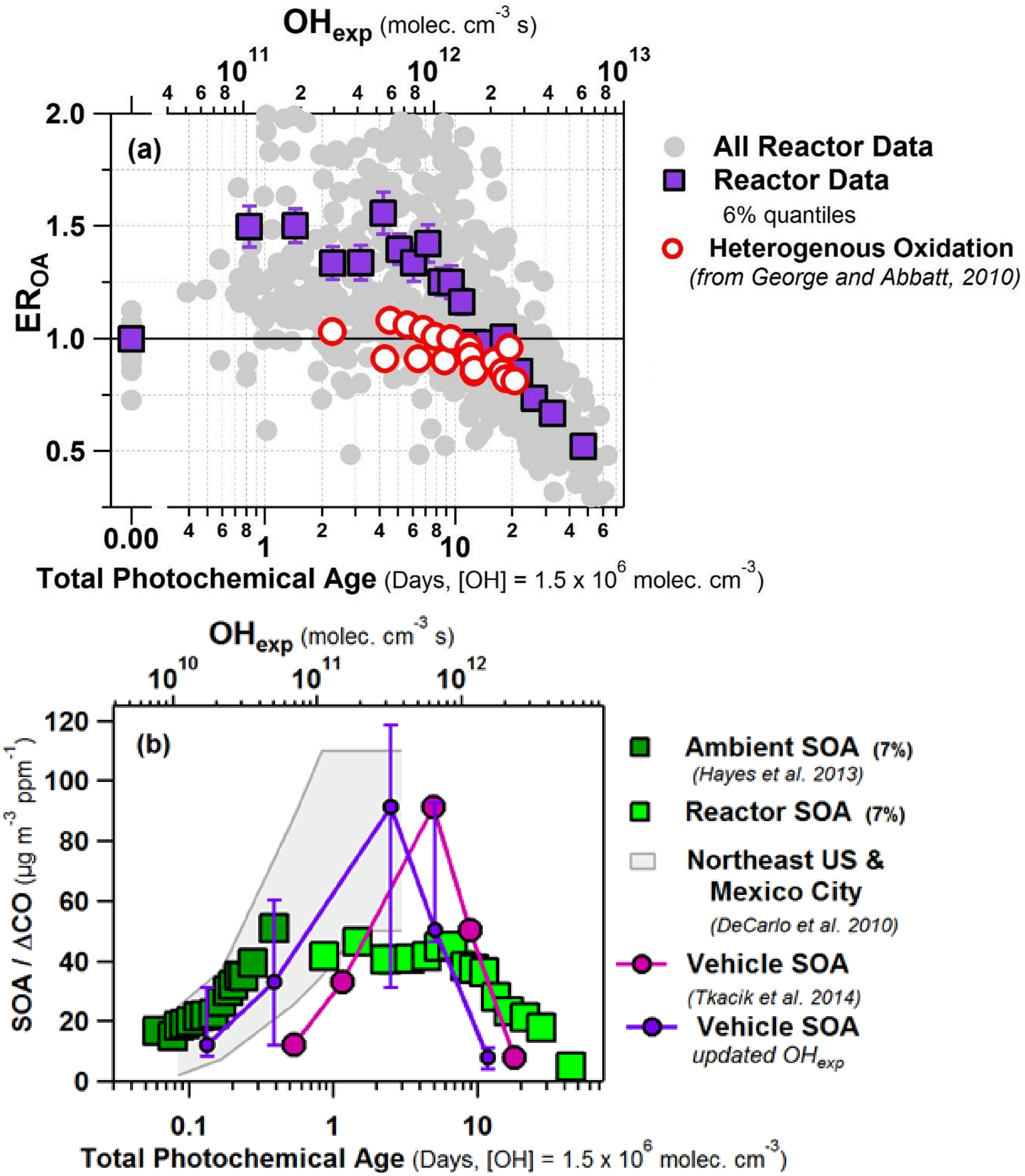

OHexp (molec. cm-3 s)
10^11
10^12
10^13
4 6 8 2 4 6 8 2 4 6 8
(a)
2.0
1.5
1.0
0.5
EROA
0.00
4 6 8
1
2 4 6 8
10
2 4 6
Total Photochemical Age (Days, [OH] = 1.5 x 10^6 molec. cm-3)
All Reactor Data
Reactor Data
6% quantiles
Heterogenous Oxidation
(from George and Abbatt, 2010)
OHexp (molec. cm-3 s)
10^10
10^11
10^12
(b)
120
100
80
60
40
20
0
SOA / ΔCO (μg m-3 ppm-1)
0.1
1
10
Total Photochemical Age (Days, [OH] = 1.5 x 10^6 molec. cm-3)
Ambient SOA (7%)
(Hayes et al. 2013)
Reactor SOA (7%)
Northeast US & Mexico City
(DeCarlo et al. 2010)
Vehicle SOA
(Tkacik et al. 2014)
Vehicle SOA
updated OHexp